

Value Approximation for Two-Player General-Sum Differential Games with State Constraints

Lei Zhang¹, Mukesh Ghimire¹, Wenlong Zhang², Zhe Xu¹, Yi Ren^{1*}

Abstract—Solving Hamilton-Jacobi-Isaacs (HJI) PDEs enables equilibrial feedback control in two-player differential games, yet faces the curse of dimensionality (CoD). While physics-informed machine learning has been adopted to address CoD in solving PDEs, this method falls short in learning discontinuous solutions due to its sampling nature, leading to poor safety performance of the resulting controllers in robotics applications where values are discontinuous due to state or other temporal logic constraints. In this study, we explore three potential solutions to this problem: (1) a hybrid learning method that uses both equilibrium demonstrations and the HJI PDE, (2) a value-hardening method where a sequence of HJIs are solved with increasing Lipschitz constant on the constraint violation penalty, and (3) the epigraphical technique that lifts the value to a higher dimensional auxiliary state space where the value becomes continuous. Evaluations through 5D and 9D vehicle simulations and 13D drone simulations reveal that the hybrid method outperforms others in terms of generalization and safety performance.

Index Terms—general-sum differential game, physics-informed machine learning, safe human-robot interactions

I. INTRODUCTION

HUMAN-ROBOT interactions (HRI) become increasingly prevalent in safety-critical application domains such as transportation [1], healthcare [2], and rescue [3]. Conventionally, safety is achieved by incorporating a state constraint in a model predictive control (MPC) framework. This constraint is usually derived from a zero-sum game formulation so that the ego player avoids all system states from which the fellow player can successfully launch attacks should it be adversarial [4]. There are two limitations in this approach: First, the zero-sum setting can often be too conservative since fellow players in civil applications are not always adversarial; second, real-time MPC is required on top of value approximation of the zero-sum games, limiting the speed and quality of the player’s decision making.

To address the first limitation, it is tempting to consider HRI as general-sum differential games with state constraints and incomplete information, where players hold private information (e.g., their benign or adversarial type). In this setting, players can overcome unnecessary conservatism by updating their beliefs about each other’s type based on observations of

their previous actions. To address the second limitation, one would ideally need to obtain the value of such a game, which then enables feedback control that intrinsically satisfies the state constraints while optimizing the expected payoff, either obsoleting or at least accelerating MPC.

A theoretical challenge towards these idealistic goals, however, is that we do not have the existence proof or the characterization of values for general-sum differential games with incomplete information and state constraints [5]. Hence we take a step back and consider games with *complete information*, for which values are proved to exist and governed by Hamilton-Jacobi-Isaacs (HJI) equations. Computing values, however, is known to encounter the curse of dimensionality (CoD) using conventional mesh-based dynamic programming [6]. Physics-informed machine learning (PIML), all called physics-informed neural network (PINN), has thus been introduced to approximate values while circumventing CoD [7]. Nonetheless, recent studies showed that while PIML is successful at approximating Lipschitz continuous PDE solutions [7]–[9], they encounter convergence issues when applied to discontinuous ones. In the context of HJI, such value discontinuity arises when state constraints are imposed.

Within this context, our paper investigates three PIML-based solutions for approximating values of state-constrained differential games:

The first solution, called *hybrid learning*, is developed based on the insight that discontinuity in value causes sampling-based methods such as PIML to diverge almost surely. The solution is thus to augment PIML with supervised equilibrium data that cover discontinuous regions of the value landscape in space and time. These equilibria are generated by solving boundary value problems (BVPs) following Pontryagin’s Maximum Principle (PMP) [10]. This solution requires human insights on what initial game states will lead to state trajectories with discontinuous values (e.g., collisions).

The second solution, called *value hardening*, is developed based on the observation that discontinuity causes the loss of spatiotemporal causality during value approximation. To this end, we followed the idea of curriculum learning [11] by gradually increasing the Lipschitz constant of a state violation penalty.

The third solution, called *epigraphical learning*, is developed based on the epigraphical technique that transforms discontinuous values of state-constrained games into Lipschitz continuous ones defined in an augmented state space [12]. We extend the existing technique from zero-sum games to general-sum ones and apply PIML to approximate the smooth augmented values.

¹Lei Zhang, Mukesh Ghimire, Zhe Xu, and Yi Ren are with Department of Mechanical and Aerospace Engineering, Arizona State University, Tempe, AZ, 85287, USA. Email:{lzhan300, mghimire, xzhe1, yiren}@asu.edu.

²Wenlong Zhang is with School of Manufacturing Systems and Networks, Ira A. Fulton Schools of Engineering, Arizona State University, Mesa, AZ, 85212, USA. Email:wenlong.zhang@asu.edu.

*Yi Ren is the corresponding author.

We evaluate and compare these potential solutions using two sets of simulation studies:

The first set is based on an uncontrolled intersection scenario where the two players can have complete or incomplete information. Here, value functions are defined on a 5-dimensional joint space of states and time, and parameterized by the player types. In the incomplete-information setting, players can be either aggressive (smaller perceived unsafe zone) or non-aggressive. By enumerating over combinations of player types and approximating values of the resultant complete-information games, players can then use the approximated values to update their beliefs about each other's type and adapt their control policies according to their beliefs. To further understand how state dimensionality and nonlinear dynamics affects the efficacy of value approximation methods, we use a second set of studies on narrow road collision avoidance and double lane change, where the values are 9- and 13-dimensional.

We claim the following contributions:

(1) We empirically show that given the same computational budget, the hybrid learning method outperforms other learning methods presented in this paper in terms of generalization performance in value prediction and safety performance when the approximated value functions are used for feedback control. We also show that hybrid learning scales better than value hardening and the epigraphical technique, as the latter struggle to generalize in higher-dimensional cases under the same computational budget.

(2) Our extensive ablation studies highlight the importance of choosing appropriate neural activation functions for value approximation, supplementing recent findings in PIML literature [13], [14]. Specifically, we found that `relu` does not generalize well due to its discontinuous derivative, while the performance of `sin` varies across different case studies. `tanh` and the continuously differentiable variants of `relu`, such as `gelu` [15], demonstrate good generalization performance when used in the hybrid method. These findings challenge the existing literature that recommends the use of `sin` for value approximation [16] and demonstrate the need for adaptive activation functions in neural network-based PDE solvers [17].

(3) While existing studies on solving HJ equations using machine learning have shown promising results for reachability analysis (e.g., [16]), the safety performance of the resultant value networks when used as closed-loop controllers is rarely investigated. To our best knowledge, this paper is the first to expose the potential risks of using value networks for closed-loop control even when they approximate backward reachable sets (i.e., unsafe zones) to high accuracy.

This paper is extended from a conference paper [18] with the following new contents: (1) we added the full investigation on epigraphical learning, the results of which are integrated into case studies and all numerical comparisons; (2) we added new empirical studies to further demonstrate and explain the convergence challenges encountered when applying value hardening to higher-dimensional cases; lastly, (3) we added Case Studies 3 and 4 to further investigate the efficacy of hybrid learning in solving 9- and 13-dimensional value approximation problems, the results of which strengthened our

conclusions.

The rest of this paper is organized as follows. Section II provides an overview of the relevant literature on value approximation, physics-informed machine learning, and complete- and incomplete-information differential games. In Section III, we present the formulation of two-player general-sum differential games with state constraints, its HJ PDEs, and explain the challenge in approximating its discontinuous values through a toy case. We then discuss the three potential solutions. The experimental results are presented and analyzed in Section IV. Finally, we conclude the paper with a discussion of possible future directions in Section V.

II. RELATED WORK

A. Value approximation and physics-informed machine learning

The values of a general-sum differential game with two-players and complete-information are viscosity solutions to HJI equations [19], which are a set of first-order nonlinear PDEs. The conventional approach to solving such equations involves essentially nonoscillatory (ENO) schemes [20] and level set methods [21], [22], which are known to provide accurate approximations of both temporal and spatial derivatives. However, these approaches suffer from CoD [23]. Recent studies have shown that using physics-informed machine learning (PIML) to approximate PDE solutions can effectively circumvent the CoD due to its Monte Carlo nature, provided that the solution is smooth [7]. PIML trains neural nets as PDE-governed fields, where the training loss is defined by network-induced residuals with respect to (a) the boundary conditions [24], [25], (b) the governing equations [16], [17], and/or (c) supervisory data drawn from the ground-truth solutions [26]. Initial studies on convergence and generalization performance have emerged for (a) and (b), under the assumption that both the solution and the network are Lipschitz continuous [8], [9], [24], but not yet for (c). Recent studies have explored the effectiveness of PIML for solving PDEs with discontinuous solutions, such as Burgers' equation, where both initial and terminal boundaries are specified [17]. However, we demonstrate in Section III-E that PDEs with only terminal or initial boundary conditions, such as HJIs, present an unidentifiability issue.

B. Differential games with incomplete information

One driving motivation for approximating values of differential games is to use the values for fast belief updates on unknown player types (e.g., preferences and intents) in incomplete-information settings. The update follows Bayes inference and relies on modeling player control policies as a type-conditioned distribution shaped by their values (see Section IV-A for details). In the case study on uncontrolled intersection (Section IV-A), we evaluate the safety performance induced by the value networks, which influence both players' control policies and their belief updates about the types of their fellow players. In addition, we examine safety performance when players are "empathetic", i.e., when they share common beliefs about each other, and when they are "non-empathetic",

i.e., when they falsely assume that their true types are known by their fellow players. Our study shares the same motivation as [27] in that both seek fast computation of equilibrium during interactions. We take the approach of pre-computing values offline, while [27] proposes to simplify games as linear-quadratic which then facilitates fast equilibrium approximation online. Our investigation into differential games with incomplete information sets us apart from previous HRI studies that resort to various simplifications of the games in order to balance theoretical soundness and practicality. These simplifications involve modeling the games as optimal control problems or complete-information ones [28]–[33]. While some also use belief updates to adapt motion planning, they are limited to empirical best responses of the uninformed player in one-sided information settings [34]–[39]. However, we study cases where both players lack information.

It is necessary to point out that we will only investigate best-response policies of players, i.e., the players choose the best responses based on their *current* belief about their fellows (via their common knowledge about the values of the games) without considering the *future* dynamics of beliefs. This is because the existence of value and player policies for general-sum differential games with incomplete information are still open questions, unlike their zero-sum counterparts [40]–[43].

III. DISCONTINUOUS VALUE APPROXIMATION

A. Notations

In a two-player differential game with complete information, Player i has a state space $\mathcal{X}_i \subset \mathbb{R}^n$ and an action space $\mathcal{U}_i \subset \mathbb{R}^m$. The time-invariant state dynamics of Player i is denoted by

$$\dot{x}_i = f_i(x_i, u_i), \quad (1)$$

where $x_i \in \mathcal{X}_i$ and $u_i \in \mathcal{U}_i$. We omit dependence on time whenever possible and use $\mathbf{a}_i = (a_i, a_{-i})$ to concatenate variables a_i from Player i and a_{-i} from the fellow player. We denote the partial derivative with respect to x by ∇_x and the joint state space by $\mathcal{X} := \bigcup_{i=1,2} \mathcal{X}_i$. The fixed time horizon of the game is $[0, T]$. The instantaneous loss of Player i is denoted by $l_i(\mathbf{x}_i, u_i)$ and the terminal loss $g_i(x_i)$. Feasible states from Player i 's perspective are defined by the sub-zero level set $\{\mathbf{x}_i \in \mathcal{X} \mid c_i(\mathbf{x}_i) \leq 0\}$. We will consider $c_i(\cdot)$ a scalar function that measures the worse state constraint violation in case multiple constraints are present, i.e., if $c_i(\mathbf{x}_i) > 0$, \mathbf{x}_i violates at least one of the constraints. The value function of Player i is denoted by $\vartheta_i(\mathbf{x}_i, t) : \mathcal{X} \times [0, T] \rightarrow \mathbb{R}$. To simplify notation, we will use f_i , l_i , g_i , c_i , and ϑ_i to refer to the dynamics, losses, state constraint, and the value function of Player i . Denote by $\alpha_i \in \mathcal{A} : \mathcal{X} \times [0, T] \rightarrow \mathcal{U}_i$ Player i 's control policy, where the policy space \mathcal{A} is assumed to be common. We use $x_s^{x_i, t, \alpha_i}$ as the state of Player i at time s if it follows policy α_i and dynamics f_i and starts at (x_i, t) . $\mathbf{x}_s^{x_i, t, \alpha_i, \alpha_{-i}} := (x_s^{x_i, t, \alpha_i}, x_s^{x_{-i}, t, \alpha_{-i}})$.

B. Assumptions

Throughout the paper, we assume that \mathcal{U}_i is compact and convex; $f_i : \mathcal{X}_i \times \mathcal{U}_i \rightarrow \mathbb{R}^n$ and $c_i : \mathcal{X} \rightarrow \mathbb{R}$ are Lipschitz

continuous; $l_i : \mathcal{X}_i \times \mathcal{U}_i \rightarrow \mathbb{R}$ and $g_i : \mathcal{X}_i \rightarrow \mathbb{R}$ are Lipschitz continuous and bounded.

C. Preliminary

Hamilton-Jacobi-Isaacs equations: Let (α_i, α_{-i}) be a pair of equilibrium policies. The values for a two-player general-sum differential game are viscosity solutions to the HJI equations denoted by (L) in Eq. (2), and satisfy the boundary conditions denoted by (D) [44].

$$\begin{aligned} L(\vartheta_i, \nabla_{\mathbf{x}_i} \vartheta_i, \mathbf{x}_i, t, \xi_{-i}) &:= \nabla_t \vartheta_i + \max_{u \in \mathcal{U}_i} \{\nabla_{\mathbf{x}_i} \vartheta_i^T \mathbf{f}_i - l_i\} = 0 \\ D(\vartheta_i, \mathbf{x}_i) &:= \vartheta_i(\mathbf{x}_i, T) - g_i = 0, \quad \text{for } i = 1, 2. \end{aligned} \quad (2)$$

With the values, the players' equilibrium policies can then be derived by $\alpha_i(\mathbf{x}_i, t) = \arg \max_{u \in \mathcal{U}_i} \{\nabla_{\mathbf{x}_i} \vartheta_i^T \mathbf{f}_i - l_i\}$. Notice that L for Player i depends on the equilibrium policy α_{-i} of its fellow.

Pontryagin's Maximum Principle: Although solving the HJI equations would give a feedback control policy, it is often more practical to compute open-loop policies for a specific initial state $(\bar{x}_1, \bar{x}_2) \in \mathcal{X}$ by solving a boundary value problem (BVP) following Pontryagin's Minimum Principle (PMP)¹:

$$\begin{aligned} \dot{x}_i &= f_i, \quad x_i(0) = \bar{x}_i, \\ \dot{\lambda}_i &= -\nabla_{x_i} h_i, \quad \lambda_i(T) = -\nabla_{x_i} g_i, \\ u_i &= \arg \max_{u \in \mathcal{U}_i} \{h_i\} \quad \text{for } i = 1, 2. \end{aligned} \quad (3)$$

Here λ_i is the time-dependent co-state for Player i . The co-state connects PMP and HJI through $\lambda_i = \nabla_{x_i} \vartheta_i$. Solutions to Eq. (3) are specific to the given initial states.

State-constrained value function: With state constraints, the value function for Player i with some equilibrium policy α_i is

$$\vartheta_i(\mathbf{x}_i, t) = \int_t^T l_i(x_s^{x_i, t, \alpha_i}, \alpha_i(x_s^{x_i, t, \alpha_i, \alpha_{-i}}, s)) ds + g_i(x_T^{x_i, t, \alpha_i}), \quad (4)$$

if $c_i(x_s^{x_i, t, \alpha_i, \alpha_{-i}}) \leq 0, \forall s \in [t, T]$, or $+\infty$ otherwise. Thus state constraints introduce discontinuity in the value landscape.

D. PIML for solving HJ equation

This section describes an approach that trains neural networks $\hat{\vartheta}_i(\cdot, \cdot) : \mathcal{X} \times [0, T] \rightarrow \mathbb{R}$ to approximate ϑ_i . We denote by $\mathcal{D} = \left\{ \left(x_1^{(k)}, x_2^{(k)}, t^{(k)} \right) \right\}_{k=1}^K$ a dataset consisting of uniform samples in $\mathcal{X}_1 \times \mathcal{X}_2 \times [0, T]$. The formulation of the training problem in Eq. (5) extends from PIML for solving zero-sum games [16]:

$$\begin{aligned} \min_{\hat{\vartheta}_1, \hat{\vartheta}_2} L_1(\hat{\vartheta}_1, \hat{\vartheta}_2; \theta) &:= \sum_{k=1}^K \sum_{i=1}^2 \left\| L(\hat{\vartheta}_i^{(k)}, \nabla_{\mathbf{x}_i} \hat{\vartheta}_i^{(k)}, \mathbf{x}_i^{(k)}, t^{(k)}) \right\| \\ &\quad + C_1 \phi \left(D(\hat{\vartheta}_i, \mathbf{x}_i^{(k)}) \right), \end{aligned} \quad (5)$$

where $\hat{\vartheta}_i^{(k)}$ is an abbreviation for $\hat{\vartheta}_i(\mathbf{x}_i^{(k)}, t^{(k)})$ and C_1 balances the PDE residual loss ($\|L\|$) and the boundary loss

¹It should be noted that solving the BVP has its own numerical challenges, particularly when the equilibrium involves singular arcs [45]. However, these challenges are beyond the scope of this paper.

($\phi(D)$). It is worth noting that in each iteration of solving Eq. (5), a sub-routine is needed to find the control policies by maximizing the Hamiltonian.

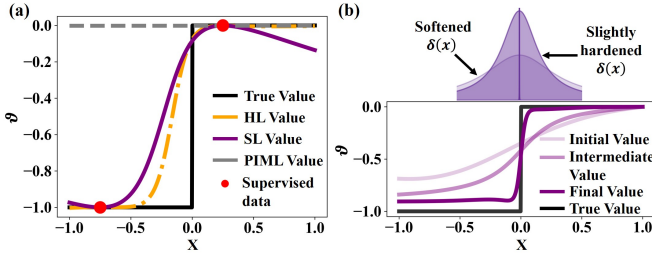


Figure 1: (a) Value comparison among the learning methods for a simple 1D case. Red dots are the supervised data. (b) Evolution of the value function due to gradually hardening delta function. Delta functions are shown on top. Transparency reduces with hardening.

E. Challenge in approximating discontinuous HJI values

We use the following toy case to explain the challenge in approximating discontinuous values using PIML. Consider a one-dimensional function $\vartheta(x)$, which is the solution to a differential equation $\nabla_x \vartheta - \delta(x) = 0$ with the boundary condition $\vartheta(1) = 0$ in the interval $x \in [-1, 1]$. $\delta(x)$ is a delta function that peaks at $x = 0$. Notice that with uniform samples for \mathcal{D} , the PIML loss (L_1) can be minimized almost surely by incorrect solutions, e.g., $\hat{\vartheta}(x) = 0$. This unidentifiability issue is due to the differential nature of the governing equation: the accuracy of $\hat{\vartheta}$ at one point in space and time depends solely on that of its neighbors. However, informative neighbors, i.e., those at $x = 0$ in this toy case, have zero probability to be sampled.

F. Solutions

(1) *Hybrid learning*: In the above toy case, we can learn a much improved approximation to the solution using only two informative data points sampled from each side of 0 (as shown by the SL curve in Fig. 1). Indeed, [26] showed that supervised learning can be used for value approximation. A drawback of this approach, when applied to solving HJIs, is its high data acquisition costs due to the need for solving BVPs to acquire state-value pairs. We hypothesize that this drawback can be reduced by combining supervised learning and PIML, since evaluating and differentiating the latter only require one forward pass of $\hat{\vartheta}$, which is usually much cheaper than calling the Newton-type iterative algorithms involved in solving BVPs.

To implement this hybrid method, we define a dataset $\mathcal{D}_s = \left\{ \left(\mathbf{x}_i^{(k)}, t^{(k)}, \vartheta_i^{(k)}, \nabla_{\mathbf{x}_i} \vartheta_i^{(k)} \right) \text{ for } i = 1, 2 \right\}_{k=1}^K$ derived from solving Eq. (3) with initial states uniformly sampled in \mathcal{X} . We define the supervised loss as follows:

$$L_2(\hat{\vartheta}_1, \hat{\vartheta}_2; \mathcal{D}_s) := \sum_{k=1}^K \sum_{i=1}^2 \left| \hat{\vartheta}_i^{(k)} - \vartheta_i^{(k)} \right| + C_2 \left\| \nabla_{\mathbf{x}_i} \hat{\vartheta}_i^{(k)} - \nabla_{\mathbf{x}_i} \vartheta_i^{(k)} \right\|, \quad (6)$$

where C_2 is a hyperparameter that balances the losses on value and its gradient. The hybrid method minimizes $L_1 + L_2$.

(2) *Value hardening*: The second solution is to introduce a surrogate differential equation, which has a continuous solution that approximates the ground truth. We can then approximate the true solution by gradually “hardening” this surrogate. For the toy case, we can improve the solution by gradually hardening a softened delta function, as shown in Fig. 1b. Just like hybrid learning, this method also introduces additional computation, as we turn one learning problem into a sequence of easier learning problems. In Section IV, we show that with a limited budget, value hardening fails to converge for high-dimensional value approximation tasks where hybrid learning succeeds. Lastly, we note that value hardening is similar to [46], where the authors introduce a gradually hardening diffusion term to address the same discontinuity issue when solving nonlinear two-phase hyperbolic transport equations using PIML.

(3) *Epigraphical learning*: Recall that the discontinuity of value in our context is caused by state constraints in differential games. It is shown that a smooth augmented value can be derived through the epigraphical technique for state-constrained differential games [12], [47]. Our last approach utilizes this technique to facilitate continuous value approximation in an augmented state space and compute the value for the original game based on the approximation. While HJ PDEs with state constraint have been investigated in zero-sum settings and numerical approximation of their values have been attempted via dynamic programming and conservative Q-learning [47], [48], this paper is among the first to solve general-sum differential games with state constraints using a combination of PIML and the epigraphical technique. For completeness, we briefly introduce the epigraphical technique in the following subsection.

G. The epigraphical technique for general-sum differential games with state constraints

Let (α_1, α_2) be a pair of equilibrium policies. The epigraphical technique introduces an augmented value $V_i : \mathcal{X} \times \mathbb{R} \times [0, T]$:

$$V_i(\mathbf{x}_i, z_i, t) := \max \left\{ \max_{s \in [t, T]} c_i(\mathbf{x}_s^{\mathbf{x}_i, t, \alpha_i, \alpha_{-i}}), g_i(x_T^{\mathbf{x}_i, t, \alpha_i}) - z_i(T) \right\} \quad (7)$$

The auxiliary state z_i follows

$$\dot{z}_i = -l_i(x_i, u_i) \text{ and } z_i(0) = \bar{z}_i, \quad (8)$$

where \bar{z}_i represents the true value of Player i at $(\bar{\mathbf{x}}_i, t_0) \in \mathcal{X} \times [0, T]$ and is computed as follows: Find $\bar{z}_i \in [z_{min}, z_{max}]$ such that $V_i(\bar{\mathbf{x}}_i, \bar{z}_i, t_0) = 0$. If $V_i(\bar{\mathbf{x}}_i, z, t_0) > 0$ for all $z \in [z_{min}, z_{max}]$, then $\bar{z}_i = +\infty$. Lemma 1 (Lemma 1 of [47]) formally establishes this connection between the augmented value V_i and the true value $\vartheta_i(\mathbf{x}_i, t)$:

Lemma 1. *Suppose assumptions in Sec. III-B hold. For all $(\mathbf{x}_i, z_i, t) \in \mathcal{X} \times \mathbb{R} \times [0, T]$, ϑ_i and V_i are related as follows:*

$$\begin{aligned} \vartheta_i(\mathbf{x}_i, t) - z_i \leq 0 &\iff V_i(\mathbf{x}_i, z_i, t) \leq 0; \\ \vartheta_i(\mathbf{x}_i, t) = \min z_i &\text{ s.t. } V_i(\mathbf{x}_i, z_i, t) \leq 0. \end{aligned} \quad (9)$$

Proof. See Appendix A.

Lemma 2 (Lemma 2 of [47]) provides the optimality condition for $V_i(\mathbf{x}_i, z_i, t)$, which is the basis for the derivation of HJ equations with state constraints.

Lemma 2. *Suppose assumptions in Sec. III-B hold. For all $(\mathbf{x}_i, z_i, t) \in \mathcal{X} \times \mathbb{R} \times [0, T]$, for small enough $h > 0$ such that $t + h \leq T$ we have*

$$V_i(\mathbf{x}_i, z_i, t) = \min_{\alpha_i \in \mathcal{A}} \max \left\{ \max_{s \in [t, t+h]} c_i(\mathbf{x}_s^{\mathbf{x}_i, t, \alpha_i, \alpha_{-i}}), \right. \\ \left. V_i(\mathbf{x}_i(t+h), z_i(t+h), t+h) \right\}, \quad (10)$$

where $\mathbf{x}_s^{\mathbf{x}_i, t, \alpha_i, \alpha_{-i}}$ and $\mathbf{x}_i(t+h)$ are solutions to Eq. (1) using (\mathbf{x}_i, t, u_i) and $z_i(t+h)$ is a solution to Eq. (8). α_{-i} is the equilibrium policy of the fellow player.

Proof. See Appendix B.

Theorem 1 presents the HJ equations for players in a general-sum differential game with state constraints:

Theorem 1 (HJ PDE with state constraints for general-sum differential games). *For all $(\mathbf{x}_i, z_i, t) \in \mathcal{X} \times \mathbb{R} \times [0, T]$, $V_i(\mathbf{x}_i, z_i, t)$ in Eq. (7) is the unique viscosity solution to the following HJ PDE and boundary conditions:*

$$\max \{ c_i(\mathbf{x}_i) - V_i(\mathbf{x}_i, z_i, t), \\ \nabla_t V_i - \mathcal{H}_i(\mathbf{x}_i, z_i, \nabla_{\mathbf{x}_i} V_i, \nabla_{z_i} V_i, t) \} = 0, \quad (11)$$

where \mathcal{H}_i is the augmented Hamiltonian:

$$\mathcal{H}_i = \max_{u_i \in \mathcal{U}_i} -\nabla_{\mathbf{x}_i} V_i^T \mathbf{f}_i + \nabla_{z_i} V_i^T l_i, \quad (12)$$

and $V_i(\mathbf{x}_i, z_i, T) = \max \{ c_i(\mathbf{x}_i), g_i(T) - z_i(T) \}$.

Proof. See Appendix C.

To solve state-constrained HJ PDEs using PIML, we define residuals similar to Eq. (2).

$$\tilde{L}(V_i, \mathbf{x}_i, z_i, t) := \max \{ c_i(\mathbf{x}_i) - V_i(\mathbf{x}_i, z_i, t), \\ \nabla_t V_i - \mathcal{H}_i(\mathbf{x}_i, z_i, \nabla_{\mathbf{x}_i} V_i, \nabla_{z_i} V_i, t) \} \\ \tilde{D}(V_i, \mathbf{x}_i, z_i) := V_i(\mathbf{x}_i, z_i, T) - \max \{ c_i(\mathbf{x}_i), \\ g_i(T) - z_i(T) \}, \text{ for } i = 1, 2. \quad (13)$$

Thus, the overall loss can be expressed using the same formulation as in Eq. (5).

$$\min_{\hat{V}_1, \hat{V}_2} L_3(\hat{V}_1, \hat{V}_2; \theta) := \sum_{k=1}^K \sum_{i=1}^2 \left\| \tilde{L}(\hat{V}_i^{(k)}, \mathbf{x}_i^{(k)}, z_i^{(k)}, t^{(k)}) \right\| \\ + C_3 \tilde{\phi} \left(\tilde{D}(\hat{V}_i^{(k)}, \mathbf{x}_i^{(k)}, z_i^{(k)}) \right), \quad (14)$$

To take advantage of the structure of V_i , we introduce two networks $A_i : \mathcal{X} \times [0, T] \rightarrow \mathbb{R}$ and $B_i : \mathcal{X} \times [0, T] \rightarrow \mathbb{R}$:

$$\hat{V}_i(\mathbf{x}_i, z_i, t) := \max \{ A_i(\mathbf{x}_i, t), B_i(\mathbf{x}_i, t) - z_i \}. \quad (15)$$

Essentially, A_i predicts the worse-case future constraint violation and B_i predicts the value of the game for Player i without considering the constraint. If $A_i > 0$, then $\hat{V}_i > 0$ and ϑ does not exist, i.e., state constraint cannot be satisfied.

IV. CASE STUDY

We conduct empirical studies to compare the generalization and safety performance of value approximation models using five different learning methods: vanilla PIML (shortened as PIML), hybrid PIML (HL), value hardening PIML (VH), epigraphical PIML (EL), and supervised learning (SL). We use both vehicle and drone simulations to formulate the games. The first simulation involves an interaction between two players (i.e., vehicle) at an uncontrolled intersection, which leads to HJIs with coupled value functions defined on a 5D state space. We study both complete- and incomplete-information settings using this simulation. The second and third studies investigate model safety performance on a 9D state space. The former models a collision-avoidance case and the latter a double lane change case. It should be noted that our settings, in terms of the dynamical models and the state space dimensions, are similar to those of [16] and [4], yet we extend from their optimal control or zero-sum settings to general-sum differential games. The last case study on drone collision avoidance investigates model performance on a higher dimensional state space (13D) and on nonlinear dynamics.

Data acquisition. The methods under comparison involves diverse data acquisition algorithms (supervised data via iterative BVP solving and PIML data via random sampling) and learning algorithms (supervised and curriculum learning). Hence, we use the total wall-clock time for data acquisition and learning as a unified measure of the computational cost. To ensure a fair comparison, the data size for each method is chosen to keep their computational costs as close to each other as possible. Computational costs of all the case studies are summarized in Table I. To improve training convergence, we normalize the input data to lie in $[-1, 1]$.

Table I: Computational costs for all learning methods in all case studies.

Case Study No.	Computational Cost (minutes)	Learning Method				
		HL	VH	EL	SL	PIML
Case 1	Data Acquisition	83	-	-	142	-
	Model Training	110	195	600	52	195
	Total Cost	193	195	600	194	195
Case 2	Data Acquisition	250	-	-	363	-
	Model Training	165	420	840	60	420
	Total Cost	415	420	840	423	420
Case 3	Data Acquisition	250	-	-	363	-
	Model Training	180	430	880	70	430
	Total Cost	430	430	880	433	430
Case 4	Data Acquisition	500	-	-	625	-
	Model Training	210	-	-	85	716
	Total Cost	710	-	-	710	716

Network architecture. For all cases, we will present results obtained using fully-connected networks with 3 hidden layers, each comprising 64 neurons, and with `tanh`, `relu`, or `sin` activation functions. The following experimentation on network architecture were conducted but omitted to keep the paper concise: (1) Experiments on deeper and wider networks did not lead to significant improvement in generalization and safety performance, or qualitative changes to the conclusions we will present; (2) we observe that `gelu` performs similarly to `tanh` in terms of the generalization and safety performance.

Hardware. For all case studies, all methods except epigraphical learning are conducted on one workstation with 3.50GHz Xeon E5-1620 v4 CPU and four GeForce GTX 1080 Ti GPU with 11 GB memory. Due to the increased dimensionality of the augmented value in epigraphical learning, we use an A100 GPU with 40 GB memory to achieve convergence. Our empirical results suggest that epigraphical learning is not as data efficient as the hybrid method even with this advantage.

A. Case 1: uncontrolled intersection

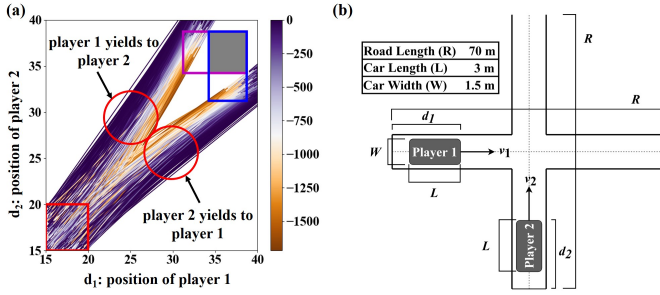


Figure 2: (a) State trajectories of players projected to (d_1, d_2) . Solid gray box: collision area from the perspective of aggressive players; hollow boxes (magenta for Player 1 and blue for Player 2): collision areas from the perspectives of non-aggressive players. Red box: sampling domain for initial states. Color: Actual values of Player 1. (b) Uncontrolled intersection setup.

Experiment setup. The schematics of the uncontrolled intersection case and the parameters (R , L , and W for road length, car length, and car width, respectively) are depicted in Fig. 2. Each player is represented by two state variables: location (d_i) and speed (v_i), which together form the state of the player as $x_i := (d_i, v_i)$. The shared dynamics between the players follow the equations $\dot{d}_i = v_i$ and $\dot{v}_i = u_i$, where $u_i \in [-5, 10]m/s^2$ represents the scalar control input, i.e., the acceleration of the player. The instantaneous loss is

$$l_i(u_i) = u_i^2, \quad (16)$$

and the player type dependent state constraint is

$$c_i(\mathbf{x}_i; \theta) = \delta(d_i, \theta_i)\delta(d_{-i}, 1) \quad (17)$$

Here $\delta(d, \theta) = 1$ iff $d \in [R/2 - \theta W/2, (R + W)/2 + L]$ or otherwise $\delta(d, \theta) = 0$. $\theta \in \Theta := \{1, 5\}$ represents the aggressive (a) or non-aggressive (na) type of a player. The terminal loss is defined to incentivize players to move across the intersection and restore nominal speed:

$$g_i(x_i) = -\mu d_i(T) + (v_i(T) - \bar{v})^2, \quad (18)$$

where $\mu = 10^{-6}$, $\bar{v} = 18m/s$, and $T = 3s$. For hybrid, value-hardening, and vanilla PIML, we treat the state constraint as a penalty in a modified instantaneous loss:

$$\tilde{l}_i(\mathbf{x}_i, u_i; \theta) = l_i(u_i) + b\sigma(d_i, \theta_i)\sigma(d_{-i}, 1), \quad (19)$$

where

$$\sigma(d, \theta) = (1 + \exp(-\gamma(d - R/2 + \theta W/2)))^{-1} (1 + \exp(\gamma(d - (R + W)/2 - L)))^{-1}, \quad (20)$$

$\gamma = 5$ is a shape parameter and $b = 10^4$ is chosen to be large enough to avoid collisions, and causes large Lipschitz constant in the resulting value functions.

Data. For supervised learning, 1.7k ground truth trajectories are generated from initial states uniformly sampled in $\mathcal{X}_{GT} := [15, 20]m \times [18, 25]m/s$ by solving Eq. (3). Each trajectory consists of 31×2 data points (sampled with a time interval of $0.1s$ and for two players), resulting in a total of 105.4k data points. For vanilla PIML and value hardening, 122k states are sampled uniformly in $\mathcal{X}_{HJ} := [15, 105]m \times [15, 32]m/s$. For hybrid learning, 1k ground truth trajectories (62k data points) are uniformly sampled in \mathcal{X}_{GT} , and 60k states are uniformly sampled in \mathcal{X}_{HJ} . For epigraphical learning, we first gather a sample of 200k states from \mathcal{X}_{HJ} to ensure adherence to the boundary conditions. Subsequently, additional 110k states are sampled from \mathcal{X}_{HJ} every 30k training iterations, resulting in a total of 1300k sampled data points upon completion of the training process.

For the auxiliary state, recall that its initial value represent the player's value of the game. In the intersection case, the best-case loss is -1.05×10^{-4} with zero collisions and control efforts, while the worst-case loss without collision is 300 where the player constantly uses the maximum acceleration or deceleration. Hence we uniformly sample $z_i \in [-1.05 \times 10^{-4}, 300]$. The same sampling procedure is applied to all sub-cases with enumeration of player types: (a, a), (na, a), (a, na), and (na, na).

The selection of state spaces to sample from, namely \mathcal{X}_{GT} and \mathcal{X}_{HJ} , is based on various factors: In the case of ground truth trajectories, the initial states for both players are uniformly sampled from identical domains. This is because informative collision and near-collision cases often occur when players start from similar states. Additionally, the range of locations for supervised data is chosen as $[15, 20]m$ to increase the likelihood of sampling informative trajectories within the specified time window. The speed range of $[18, 25]m/s$ is selected based on typical vehicle speed limits. For PIML and variants, the sample space \mathcal{X}_{HJ} approximately covers all states that players can reach within the time window. It is noteworthy that within $\mathcal{X}_{HJ} \times \mathcal{X}_{HJ}$, about 20% of the states will induce collision. Adaptive sampling for PIML such as in [17] can potentially improve the data efficiency further but is not studied in this paper.

Training. All training problems except epigraphical learning are solved using the Adam optimizer with a fixed learning rate of 2×10^{-5} . For supervised learning, the networks are trained for 100k iterations. For vanilla PIML, we adopt the curriculum learning method proposed in [16]. Specifically, we first train the networks for 10k iterations using 122k uniformly sampled boundary states at the terminal time. We then refine the networks for 260k gradient descent steps, with states sampled from an expanding time window starting from the terminal. For value hardening, we follow the same learning procedure, but we soften the collision penalty using sigmoid functions and gradually increased the shape parameter of the sigmoid to harden the penalty. To keep the computational cost of value hardening similar to that of the hybrid, we use 5.4k training iterations for each hardening step for a total of 50 steps. For the hybrid method, we pre-train the networks for 100k iterations using the supervised data and combine the supervised data with states sampled from an expanding time

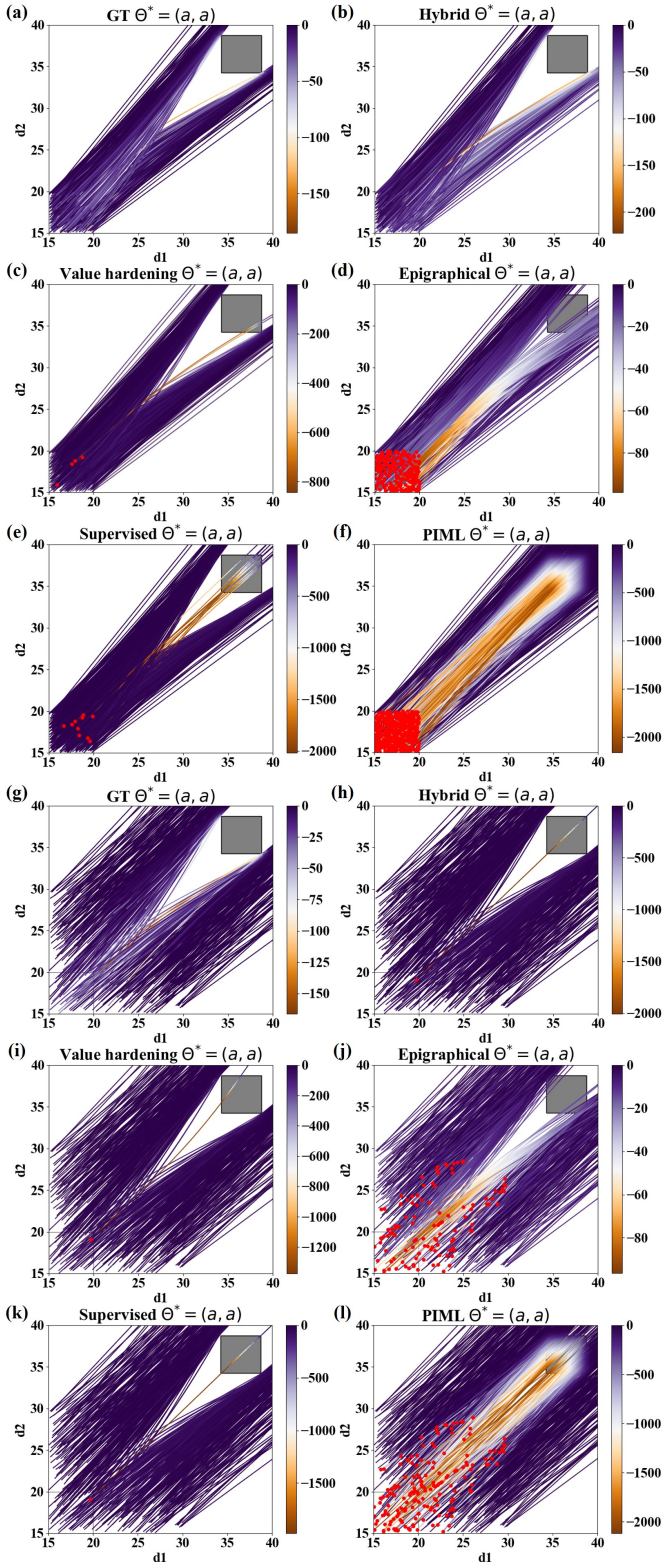


Figure 3: (a), (g): Ground truth trajectories (projected to d_1 - d_2) for \mathcal{X}_{GT} and \mathcal{X}_{XP} , respectively. (b-f), (h-l): Trajectories generated using hybrid, value hardening, epigraphical, supervised, and vanilla PIML methods under \mathcal{X}_{GT} and \mathcal{X}_{XP} , respectively. Color: Actual equilibrium values of Player 1 along the trajectories. Trajectories with inevitable collisions are removed for clearer comparison on safety performance. Red dots represent initial states with *avoidable* collisions.

window starting from the terminal time to minimize $L_1 + L_2$

for 100k iterations. For epigraphical learning, we first train the network to fulfill the boundary condition over 50k iterations. Subsequently, we refine the network through 3k gradient steps per epoch, encompassing a total of 10 epochs for every 30k training iterations. The network refinement process spans 300k training iterations in total.

It should be noted that our initial experiment with epigraphical learning led to poor generalization and safety performance. In the results we will present, adaptive activations [17] and adaptive learning rates are implemented, in addition to the use of a larger computational budget, to slightly improve the performance, which still falls short of that of hybrid learning.

Table II: Generalization and safety performance on complete-information games. HL, VH, EL, SL, PIML are for hybrid, value hardening, epigraphical, supervised, and physics-informed machine learning methods, respectively.

Test Domain	Player Types	Learning Method	Metrics		
			$ \vartheta - \hat{\vartheta} \downarrow$	$ u - \hat{u} \downarrow$	Col.% \downarrow
\mathcal{X}_{GT}	(a, a)	HL	0.46	0.09 \pm 0.10	0.00%
		VH	4.17	0.34 \pm 0.19	0.67%
		EL	8.20	0.85 \pm 3.92	42.3%
		SL	0.57	0.12 \pm 0.36	1.67%
		PIML	3.39	0.96 \pm 4.19	84.8%
	(a, na)	HL	9.43	0.49 \pm 3.55	3.50%
		VH	79.35	1.10 \pm 5.42	0.50%
		EL	22.83	2.24 \pm 20.8	42.7%
		SL	10.58	0.54 \pm 3.92	4.50%
		PIML	15.33	1.27 \pm 7.16	83.3%
(na, na)	HL	1.00	0.04 \pm 0.03	1.33%	
	VH	21.76	0.34 \pm 1.33	8.50%	
	EL	126.83	0.66 \pm 5.66	16.5%	
	SL	3.49	0.10 \pm 0.46	4.33%	
	PIML	114.67	1.88 \pm 13.72	83.5%	
\mathcal{X}_{XP}	(a, a)	HL	0.41	0.09 \pm 0.08	0.20%
		VH	2.03	0.20 \pm 0.07	0.20%
		EL	4.76	0.34 \pm 1.62	19.0%
		SL	0.69	0.17 \pm 0.28	0.20%
		PIML	1.54	0.37 \pm 1.88	35.2%
	(a, na)	HL	17.39	0.46 \pm 3.17	0.10%
		VH	32.64	0.57 \pm 2.71	0.20%
		EL	24.10	0.96 \pm 8.64	10.5%
		SL	19.01	0.56 \pm 3.09	0.60%
		PIML	19.57	0.58 \pm 3.89	31.3%
(na, na)	HL	1.80	0.10 \pm 0.12	0.00%	
	VH	11.54	0.24 \pm 0.68	6.40%	
	EL	66.57	0.41 \pm 3.02	2.33%	
	SL	4.25	0.30 \pm 0.72	2.20%	
	PIML	60.39	0.95 \pm 7.31	36.0%	

1) *Results for complete-information games:* We generate a separate set of 600 ground truth trajectories for each of the four player type configurations by solving BVPs, with initial states uniformly sampled from \mathcal{X}_{GT} . To evaluate generalization performance, we measure the mean absolute errors (MAEs) of value and control input predictions, denoted by $|\vartheta - \hat{\vartheta}|$ and $|u - \hat{u}|$, respectively, across the test trajectories. For safety performance, we use the learned value networks to compute the players' closed-loop control inputs and the state trajectories. From all resulting trajectories computed based on test initial states, we report the percentage of collisions that are *avoidable* according to BVP solutions. The performance results are summarized in Table II, where we averaged the performance of (a, na) and (na, a) due to their symmetry. Sample trajectories for (a, a) are shown in Fig. 3.

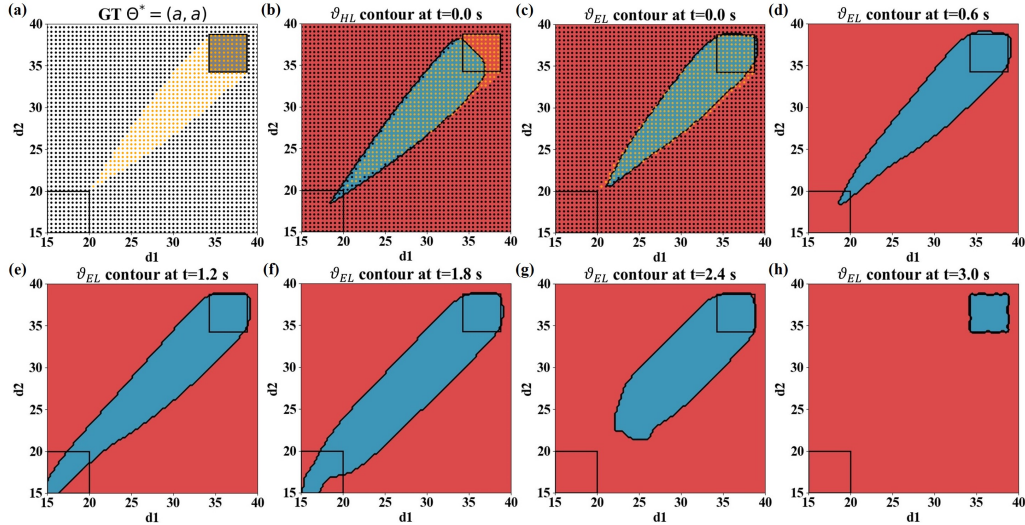


Figure 4: (a) Ground truth safe/unsafe initial states projected to d_1 - d_2 frame, where black dots represent collision-free trajectories while orange dots depict trajectories with collision. (b-h): Value contours in different time slices to classify the safe/unsafe zone using hybrid and epigraphical learning, respectively. The blue region represents the set of states that are unsafe while both players are safe in the red region. The classification results obtained through epigraphical learning align with those depicted in Figure 4a.

To further evaluate the out-of-distribution performance of supervised and hybrid learning, we repeat the tests using 500 uniformly sampled initial states in \mathcal{X}_{XP} . The results are summarized in the same table and figure. In both tests, the hybrid method demonstrates the best generalization and safety performance. Notably, the vanilla PIML exhibits poor generalization due to value discontinuity. Epigraphical learning performs only better than vanilla PIML in regard of safety. Further inspection shows that epigraphical learning can actually identify the backward reachable sets (i.e., unsafe zones) well, see Fig. 4. To elaborate, given $t \in [0, T]$ and a value network \hat{V} trained for fix player types (a, a) , the unsafe zone is defined as $\{\mathbf{x} \in \mathcal{X}_{XP} | \hat{V}(\mathbf{x}, t) > 0\}$. We approximate the ground truth unsafe zone by computing trajectories of sample initial states in \mathcal{X}_{XP} by solving Eq. (3) (Fig. 4a). We compare the ground truth with the approximations from hybrid and epigraphical learning in Fig. 4b,c. The results here reveal an important limitation of values approximated through PIML: High empirical accuracy in characterizing the unsafe zone does not necessarily imply high safety performance, such as in the case of epigraphical learning. This is potentially because feedback control requires accurate approximation of the value *gradients* instead of the segmentation of value in space-time. For the same reason, high safety performance does not imply high accuracy in characterizing the unsafe zone either, such as in the case of hybrid learning. Indeed, these two application-specific metrics are not directly used as the learning objective, although value gradients are partially considered in the formulation of PIML (see Eq. (6)). We discuss future solutions in Sec. V when associating PIML with reinforcement learning.

Ablation studies. We conduct ablation studies to understand the effects of activation functions and the norm of the boundary loss on model performance. Safety results are summarized in Table III for player types (a, a) and using the hybrid learning method, with training and testing conducted in

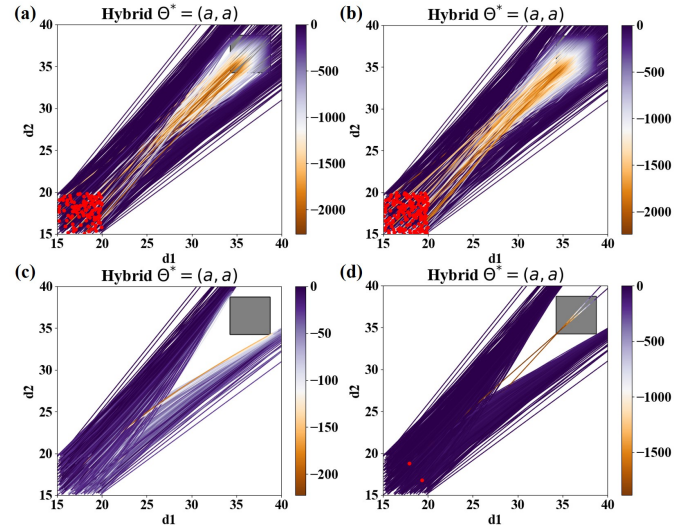


Figure 5: Trajectories generated using neural networks with (a) relu and (b) sin activation functions and using L^1 for boundary norm (for tanh , refer to Fig. 3); trajectories generated using (c) L^1 - and (d) L^2 -norms for the boundary values and using tanh for activation. All trajectories are based on hybrid learning.

Table III: Safety performance w/ different activation functions (w/ L^1) and boundary norms (w/ tanh)

Method	Activation			Boundary Norm	
	tanh	relu	sin	L^1	L^2
Hybrid	0.00%	19.8%	28.7%	0.00%	0.4%
Value hardening	0.67%	85.1%	84.6%	-	-
Epigraphical	42.3%	78.8%	89.8%	-	-
Supervised	1.67%	2.50%	19.5%	-	-
Physics-informed	84.8%	84.0%	84.7%	-	-

\mathcal{X}_{GT} . The corresponding trajectories are visualized in Fig. 5. The results indicate that (1) the choice of the activation function significantly affects the resultant models, with tanh outperforming relu and sin , and (2) the choice of the boundary norm does not have a significant influence.

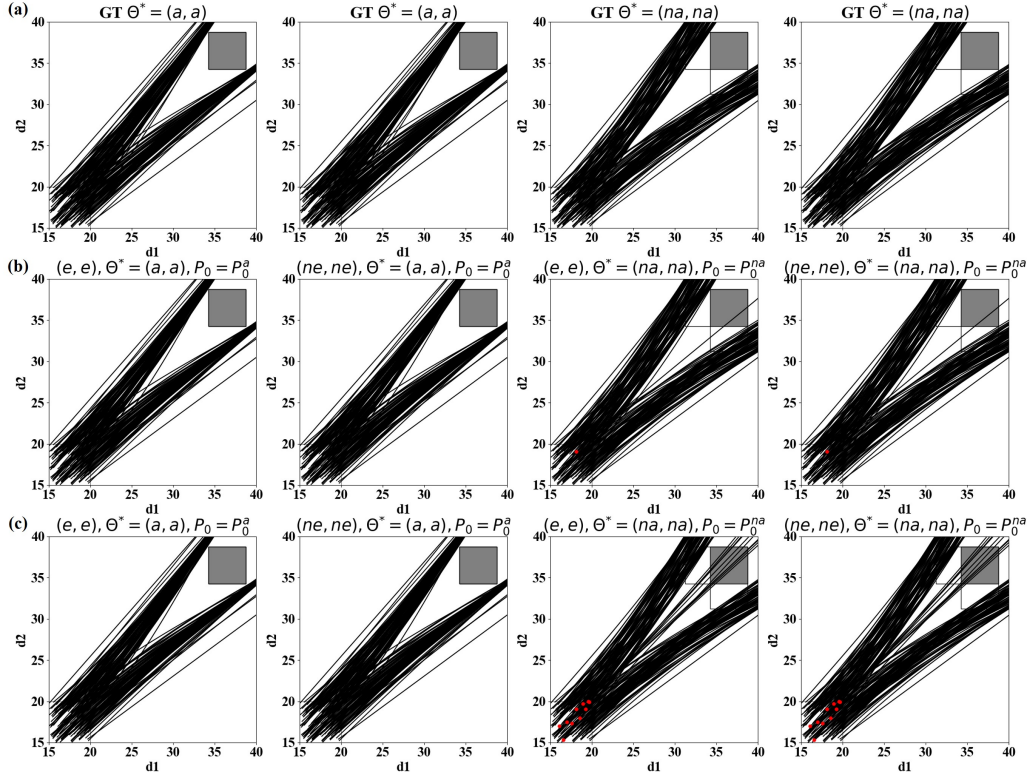


Figure 6: (a) Ground truth trajectories (projected to d_1 - d_2) for \mathcal{X}_{GT} . Trajectories generated using (b) hybrid and (c) supervised models using empathetic and non-empathetic belief update models, respectively. Here the common beliefs of players match with their true types.

Remarks: We note that `relu` networks have been shown to converge to piecewise smooth functions in a supervised setting [49]. However, convergence in the PIML setting requires continuity of the network and its gradient [8], which `relu` does not offer. Our results are consistent with those of [17], where `relu` underperforms in solving PDEs. We note, however, that smooth variants of `relu` such as `gelu` can achieve performance comparable to that of `tanh`. We also note that while `sin` does not perform well for Case 1, it achieves comparable performance to `tanh` in Cases 2-4 (see Section IV-B, IV-C and IV-D). This result suggests that fine-tuning of the frequency parameter of `sin` is necessary and case-dependent [50].

2) *Results for incomplete-information games:* In games with incomplete information, we investigate the effectiveness of using value networks both for closed-loop control and for belief updates: Each player is uncertain about the types of the other players and therefore holds a belief about their fellow player’s types. A belief is a probability distribution over the type space and is updated over time as the player observes new actions from their fellow player. We examine two belief update settings: the first assumes that players have common prior belief and synchronized belief dynamics [51]. In other words, Player i knows about Player j ’s uncertainty about Player i ’s type. We refer to players in this setting as “empathetic”. The second setting is non-empathetic, where Player i falsely assumes that Player j has full knowledge about Player i ’s type. We follow [39] to simulate the state and belief dynamics: We model Player i to continuously update its belief based on observations, and then determine its next

control inputs based on the value network parameterized by the most likely type of Player j as well as Player i ’s truth type. We evaluate the efficacy of the hybrid and supervised methods, which achieve the best performance across cases, by measuring their safety performance in incomplete-information settings. The simulations use the same initial states as tests in the complete-information games.

Empathetic belief update. We consider the case where players can take one of the two types: $\Theta = \{a, na\}$. Let $\mathcal{D}_t = \{(\mathbf{x}(k), \mathbf{u}(k))\}_{k=1}^t$ be a finite set of observed states and control inputs of both players accumulated up to time t . Let $p_i(t) := \Pr(\theta_i = a \mid \mathcal{D}_{t-1})$ be the belief of Player j about Player i at the beginning of time step t , and $q_i^{\hat{\theta}}(t) := \Pr(u_i(t) \mid \mathbf{x}(t), \hat{\theta})$ where $\hat{\theta} \in \{(a, a), (a, na), (na, a), (na, na)\}$ is a point estimate of θ based on the current beliefs \mathbf{p} . We assume Player i ’s control policy follows a Boltzmann distribution:

$$q_i^{\hat{\theta}}(t) = \frac{e^{h_i(\mathbf{x}_i(t), u_i(t), t; \hat{\theta})}}{\sum_{\mathcal{U}} e^{h_i(\mathbf{x}_i(t), u_i', t; \hat{\theta})}}, \quad (21)$$

where

$$h_i(\mathbf{x}_i(t), u_i(t), t; \hat{\theta}) = \nabla_{\mathbf{x}_i} \mathbf{f}_i^T \vartheta_i^{\hat{\theta}} - \tilde{l}_i^{\hat{\theta}}. \quad (22)$$

$\vartheta_i^{\hat{\theta}}$ is Player i ’s approximated value if the game is played with player types $\hat{\theta}$, and $\tilde{l}_i^{\hat{\theta}}$ is the instantaneous loss that incorporates the collision penalty if Player i is of type $\hat{\theta}_i$.

Denote the marginal by $q_i^{\hat{\theta}_i}(t) := \Pr(u_i(t) \mid \mathbf{x}(t), \hat{\theta}_i)$, we have

$$q_i^{\hat{\theta}_i}(t) = q_i^{(\hat{\theta}_i, a)}(t)p_{-i}(t) + q_i^{(\hat{\theta}_i, na)}(t)(1 - p_{-i}(t)). \quad (23)$$

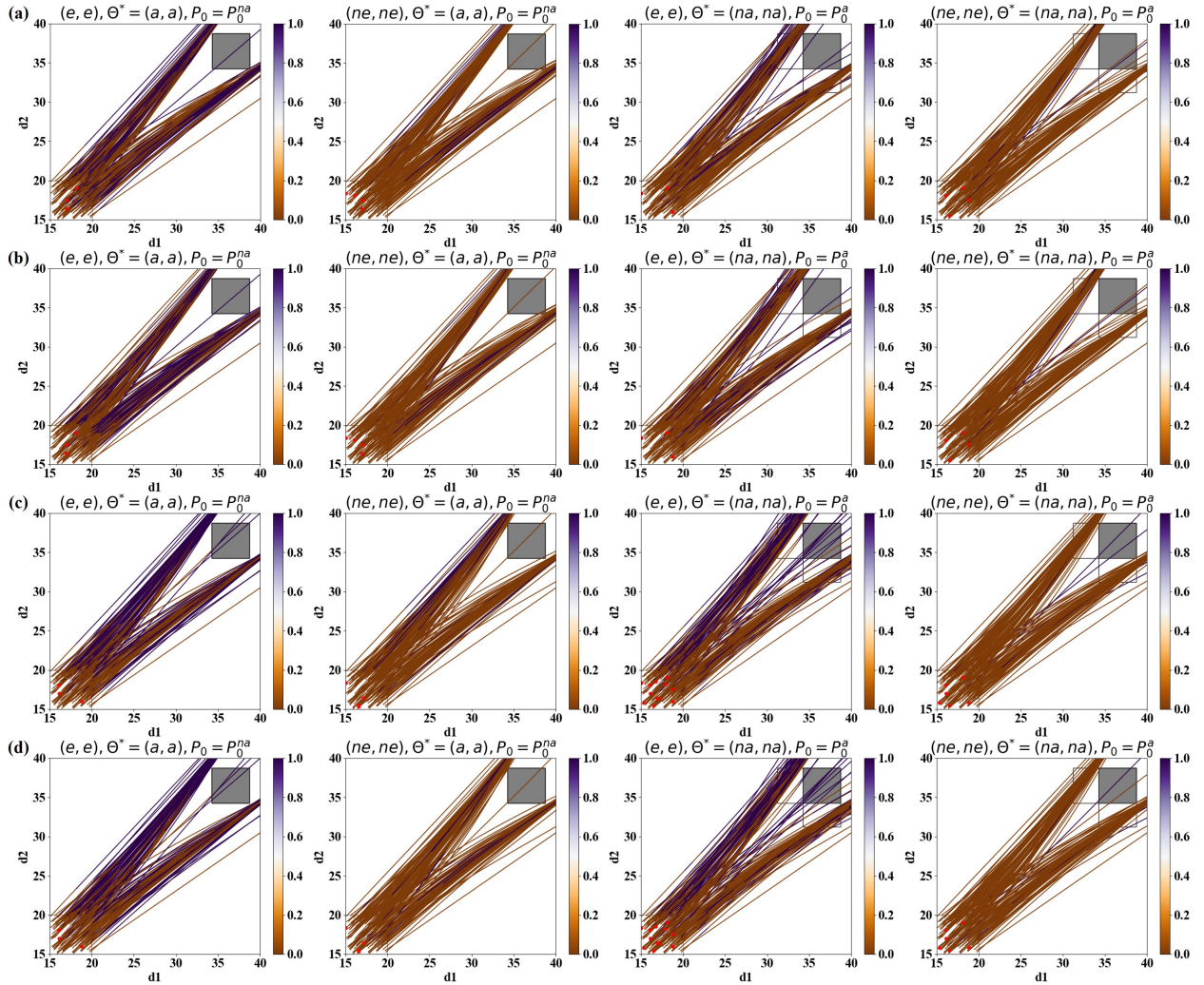


Figure 7: Interactions when common belief mismatches with true player types. Trajectories generated using hybrid models for (a) Player 1 and (b) Player 2, and using supervised models for (c) Player 1 and (d) Player 2. Color: Binary code of player's belief about other's type, 1 (purple) represents the consistency of the player's belief and the other's type while 0 (yellow) shows the lack of consistency.

Given the observations \mathcal{D}_t , p_i follows a Bayes update:

$$p_i(t+1) = \frac{q_i^a(t)p_i(t)}{q_i^a(t)p_i(t) + q_i^{na}(t)(1-p_i(t))}. \quad (24)$$

Remarks: (1) If any element of $\mathbf{p}(t)$ is mistakenly assigned a zero probability, this mistake cannot be corrected in future updates. To address this, we modify $\mathbf{p}(t)$ using

$$\mathbf{p}(t) \leftarrow (1 - \epsilon)\mathbf{p}(t) + \epsilon\mathbf{p}(0), \quad (25)$$

before its next update and set the learning rate $1 - \epsilon = 0.95$. $\mathbf{p}(0)$ represents the initial belief. (2) To make Eq. (21) more tractable, we discretize the space of control inputs as $\mathcal{U} := \{-5, -4, \dots, 0, \dots, 10\}m/s^2$. Additionally, we used discrete time steps with a time interval of 0.05 seconds to simulate the interactions. (3) We test two settings of initial beliefs. In the first setting, each player believes that the other player has a probability of 80% of being aggressive; in the second setting, the probability is 20%. These initial beliefs correspond to $\mathbf{p}(0) = (0.8, 0.2)$ and $\mathbf{p}(0) = (0.2, 0.8)$, respectively. While a more extensive test over the initial belief space could be interesting, it is beyond the scope of this study.

Non-empathetic belief update. A non-empathetic player updates its belief about the other player's type by assuming that his type is known. Let the true types be θ^* . Player $-i$'s belief about Player i 's type now becomes a conditional $p'_i(t) := \Pr(\theta_i = a | \mathcal{D}_{t-1}, \theta_{-i}^*)$. The Bayes update of $p'_i(t)$ follows:

$$p'_i(t+1) = \frac{q_i^{(a, \theta_{-i}^*)}(t)p'_i(t)}{q_i^{(a, \theta_{-i}^*)}(t)p'_i(t) + q_i^{(na, \theta_{-i}^*)}(t)(1-p'_i(t))}. \quad (26)$$

Consequently, each player starts with its own belief, which are not necessarily common during the interaction.

Control policy. Given the beliefs $p_i(t)$ or $p'_i(t)$, Player $-i$ finds the most likely type of Player i . The control policy of Player i is determined by the value function corresponding to $(\theta_i^*, \hat{\theta}_{-i})$. It is worth noting that Player i employs a policy that is consistent with its true type, even if Player j holds an incorrect belief about Player i , which Player i acknowledges in the empathetic setting. This setup allows players to signal their own types through their actions.

Simulation results. We present simulated interactions between two players at an uncontrolled intersection in an incomplete-

Table IV: Collision probabilities in uncontrolled intersections with incomplete information: e - empathetic, ne - non-empathetic

Belief update model	Initial belief	True type	Hybrid	Supervised
(e,e)	(a,a)	(a,a)	0.00%	0.00%
(ne,ne)	(a,a)	(a,a)	0.00%	0.00%
(e,e)	(na,na)	(na,na)	0.67%	6.67%
(ne,ne)	(na,na)	(na,na)	0.67%	6.67%
(e,e)	(a,a)	(na,na)	2.00%	2.67%
(ne,ne)	(a,a)	(na,na)	2.67%	2.67%
(e,e)	(na,na)	(a,a)	2.00%	8.00%
(ne,ne)	(na,na)	(a,a)	2.67%	4.00%

information setting. The simulations are performed on a grid that enumerates the following settings: (empathetic, non-empathetic) \times (correct prior, wrong prior) \times (aggressive, non-aggressive), where both players have identical settings to limit the scope. For each setting, we evaluate the safety performance of the value approximation models learned through the hybrid and supervised methods using test samples from \mathcal{X}_{GT} . The resulting trajectories for when the players have correct and incorrect priors are depicted in Fig. 6 and Fig. 7, respectively. To examine how incorrect priors can (or cannot) be corrected during the interactions, we use binary code to indicate whether the ego player has a correct or wrong belief about the fellow player's type in Fig. 7, where 1 (0) means the ego player has a correct (wrong) point estimate of the fellow's type. Our observations suggest that players with empathetic beliefs have a better chance of correcting their beliefs than non-empathetic players. Table IV summarizes the results in the figures, which show that the hybrid models have a lower chance of collision than the supervised ones under all settings.

B. Case 2: narrow road collision avoidance

Experiment setup. The schematic is depicted in Fig. 8, where the states of Player i consist of its location (p_i^x, p_i^y) , orientation (ψ_i) , and speed (v_i) , denoted as $x_i := [p_i^x, p_i^y, \psi_i, v_i]^T$. The system dynamics is modeled using a unicycle model:

$$\begin{bmatrix} \dot{p}_i^x \\ \dot{p}_i^y \\ \dot{\psi}_i \\ \dot{v}_i \end{bmatrix} = \begin{bmatrix} v_i \cos(\psi_i) \\ v_i \sin(\psi_i) \\ \omega_i \\ u_i \end{bmatrix}, \quad (27)$$

where $\omega_i \in [-1, 1]rad/s$ and $u_i \in [-5, 10]m/s^2$ are control inputs that represent angular velocity and acceleration, respectively. The instantaneous loss incorporates control effort:

$$l_i(x_i, u_i; \theta_i) = k\omega_i^2 + u_i^2, \quad (28)$$

where $k = 100$. The state constraint is:

$$c_i(\mathbf{x}_i) = \eta - \sqrt{((R - p_2^x) - p_1^x)^2 + (p_2^y - p_1^y)^2}. \quad (29)$$

where $\eta = 1.5m$ and $R = 70m$. $c_i(\cdot) > 0$ is considered as a collision incident. The parameter R represents the length of the road, and $\eta = 1.5m$ is the collision threshold. The terminal loss is designed to encourage players to move along the lane and restore nominal speed:

$$g_i(x_i) = -\mu p_i^x(T) + (v_i(T) - \bar{v})^2 + (p_i^y(T) - \bar{p}^y)^2, \quad (30)$$

where $\mu = 10^{-6}$, $\bar{v} = 18m/s$, $\bar{p}^y = 3m$, and $T = 3s$. For hybrid, value-hardening, and vanilla PIML, we treat the state constraint as a penalty in a modified instantaneous loss:

$$\tilde{l}_i(\mathbf{x}_i, \omega_i, u_i) = k\omega_i^2 + u_i^2 + b\sigma(\mathbf{x}_i, \eta), \quad (31)$$

where the penalty function is defined as

$$\sigma(\mathbf{x}_i, \eta) = (1 + \exp(-\gamma c_i(\mathbf{x}_i)))^{-1}.$$

The parameter b is set to 10^4 to impose a high penalty on collision, while $\gamma = 5$ is a shape parameter.

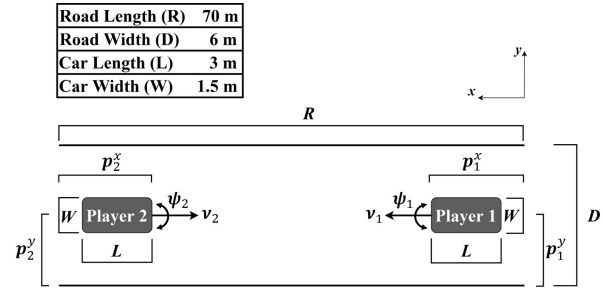


Figure 8: Narrow road collision avoidance setup with two players.

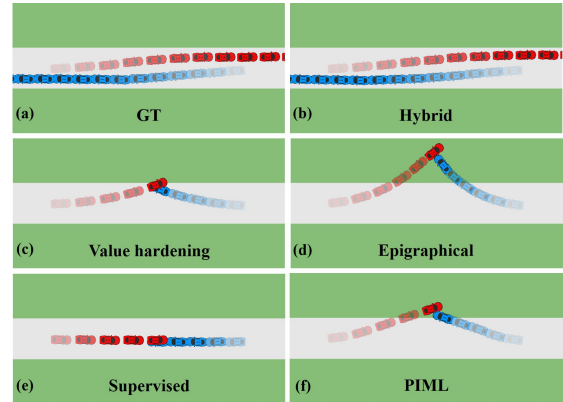


Figure 9: Narrow road collision avoidance visualization: (a): Ground truth safe trajectory. Transparency reduces along time. (b-e): Trajectories generated using hybrid, value hardening, epigraphical, supervised, and vanilla PIML models, respectively.

Data. For supervised learning, we generate 1.45k ground truth trajectories by uniformly sampling initial states from $\mathcal{X}_{GT} := [15, 20]m \times [2.25, 3.75]m \times [-\pi/180, \pi/180]rad \times [18, 25]m/s$, resulting in a total of 89.9k data points. For vanilla PIML and its value-hardening variant, we uniformly sample 122k states from $\mathcal{X}_{HJ} := [15, 90]m \times [0, 6]m \times [-0.15, 0.18]rad \times [18, 25]m/s$. For hybrid learning, we generate 1k ground truth trajectories (62k data points) by uniformly sampling initial states from $[15, 20]m \times [2.25, 3.75]m \times [-\pi/180, \pi/180]rad \times [18, 25]m/s$ and sample 60k states uniformly from $[15, 90]m \times [0, 6]m \times [-0.15, 0.18]rad \times [18, 25]m/s$. For epigraphical learning, we introduce an auxiliary state z_i with a range of $[-9 \times 10^{-5}, 300]$ to account for both the best- and worst-case scenarios. We employ the same settings as in Case 1 for the remaining aspects of the experiment.

Training. For vanilla PIML, we pretrain the networks for 10k iterations using 122k uniformly sampled boundary states

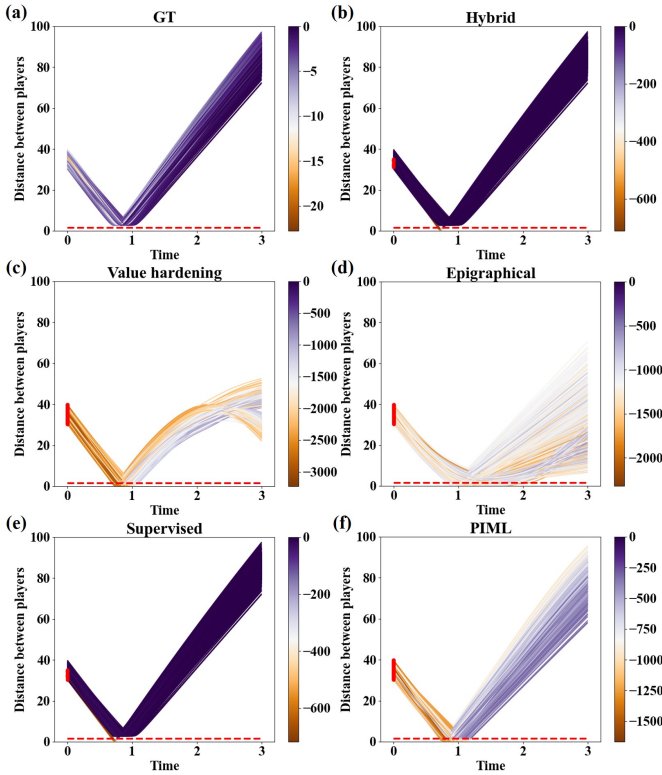
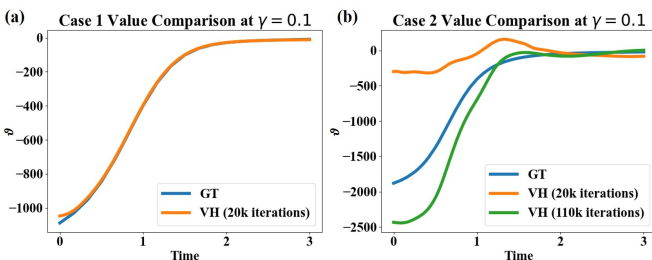


Figure 10: (a): Ground truth distance between players over time for \mathcal{X}_{GT} . (b-e): Distance between players over time using hybrid, value hardening, epigraphical, supervised, and vanilla PIML under \mathcal{X}_{GT} , respectively. Red dashed line represents the threshold distance for collision.

and then train them for 430k iterations. For value hardening, we use 8.8k training iterations for each hardening step and a total of 50 steps for a fair comparison. The remaining settings are the same as those in Case 1.

Table V: Safety performance w/ different activation functions under \mathcal{X}_{GT}

Test Domain	Activation Functions	Learning Method				
		HL	VH	EL	SL	PIML
\mathcal{X}_{GT}	tanh	1.67%	95.2%	48.3%	2.17%	81.3%
	relu	65.2%	98.2%	70.5%	67.7%	83.8%
	sine	1.67%	98.5%	69.7%	3.17%	98.3%



Model Training Time Cost	Case 1		Case 2	
	20k iterations for each hardening step	80 min	110k iterations for each hardening step	450 min

Figure 11: (a): Value hardening uses 20k training iterations for each hardening step, for a total of 10 steps to converge to ground truth in Case 1. (b) Value hardening uses 20k/110k training iterations for each hardening step, for a total of 10 steps to converge to ground truth in Case 2. Compared to Case 1, value hardening takes around 5.6 times longer to converge to the ground truth in Case 2.

Results. We evaluate the safety performance of the methods on a test set of 600 ground truth collision-free trajectories with initial states drawn from \mathcal{X}_{GT} . The results are summarized in Table V, and the distance between players during interactions is visualized in Fig.10. Similar to Case 1, the hybrid learning method outperformed the others.

We notice that value hardening fails to generalize well in this higher-dimensional case (and in Case 3). We hypothesize that vanilla PIML, which value hardening is based on, is less scalable in compute than hybrid PIML as the state dimensionality increases.

While the relationship between learning dynamics of PIML and state dimensionality is yet to be understood, here we empirically show that value hardening PIML requires significantly higher compute to converge in Case 2 due to its higher state dimensionality. To make this empirical study more tractable, we use a mildly softened collision penalty with $\gamma = 0.1$ in both Case 1 and 2. We uniformly sample 122k states from X_{HJ} and train the model using 10 hardening steps until γ reaches 0.1. To visualize the convergence, in Figure 11 we show the value along a randomly chosen equilibrium trajectory derived from PMP for Case 1 (left) and Case 2 (right). We can see that by 20k iterations, value hardening already converges to the ground truth in Case 1, while in Case 2, convergence requires more than 110k iterations.

Similar to [52], we show that poor generalization of a value network can be attributed to larger errors in its low-frequency components, the learning of which becomes harder when the state dimensionality increases. While the ground truth value is unknown and therefore cannot be used for frequency comparisons, the hybrid method has good generalization performance and will be used as a surrogate of the true value. Fig.12 compares the magnitude spectrum $F[\vartheta]$ of the value functions derived by the hybrid (left columns) and the value hardening (middle columns) methods in the frequency domain: Low-frequency components are depicted at the center, while high-frequency components are shown in the corners. The color bar represents the magnitude spectrum of $F[\vartheta]$. For Case 1, we fix all states except for (d_1, d_2) , while for Case 2 and 3, we use (p_1^x, p_2^x) . The difference $|F[\vartheta]_{HL} - F[\vartheta]_{VH}|$ is close to zero in Case 1, especially in the low-frequency domain. This, however, is not observed in Cases 2 or 3. This finding is consistent with the poor generalization and safety performance observed in Cases 2 and 3 when using value hardening.

C. Case 3: double lane change

Experiment setup. The schematic is shown in Figure 13, depicting the states of Player i as its location (p_i^x, p_i^y) , orientation (ψ_i) , and speed (v_i) . $x_i := [p_i^x, p_i^y, \psi_i, v_i]^T$. The dashed blue and orange color (with increasing transparency along the x-axis) in the figure represents desired trajectories for both players. We use the same unicycle model and instantaneous loss as in Section IV-B. The terminal loss is set to incentivize players to stay within their respective lanes and regain the nominal speed:

$$g_i(x_i) = -\mu p_i^x(T) + (p_i^y(T) - \bar{p}_i^y)^2 + (v_i(T) - \bar{v})^2 + \kappa(\psi_i(T) - \bar{\psi})^2, \quad (32)$$

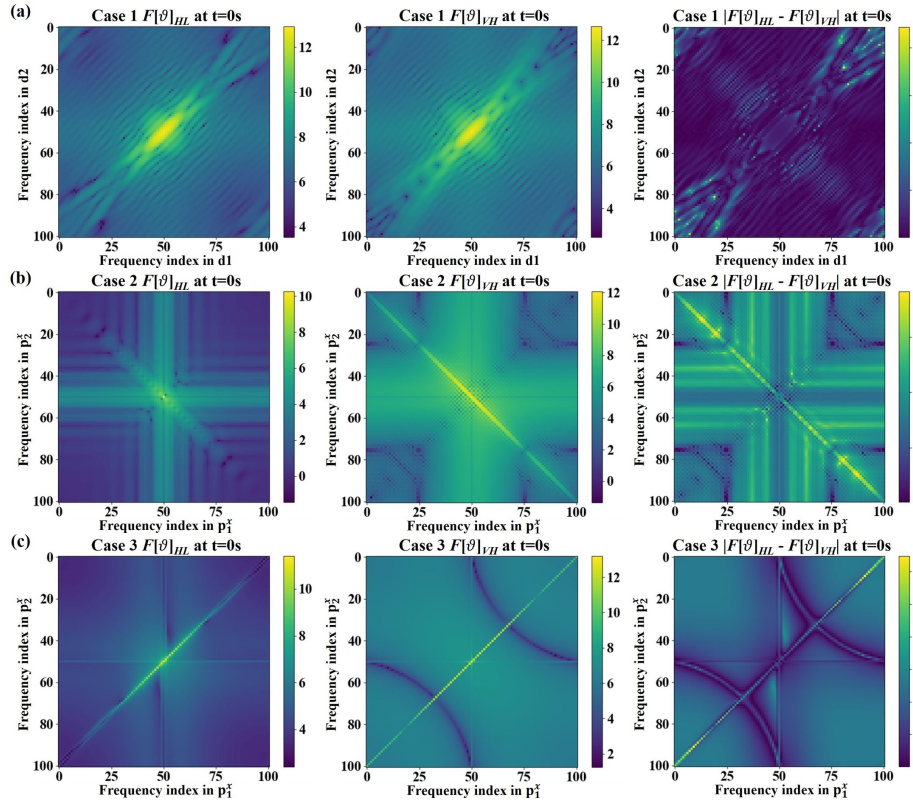


Figure 12: (a): Fourier transform $F[\vartheta]$ using hybrid and value hardening models and the difference $|F[\vartheta]_{HL} - F[\vartheta]_{VH}|$ in frequency domain given fixed states except for (d_1, d_2) in Case 1 at $t=0$. (b,c) Fourier transform $F[\vartheta]$ using hybrid and value hardening models and the difference $|F[\vartheta]_{HL} - F[\vartheta]_{VH}|$ in frequency domain given fixed states except for (p_1^x, p_2^y) in Case 2-3 at $t=0$.

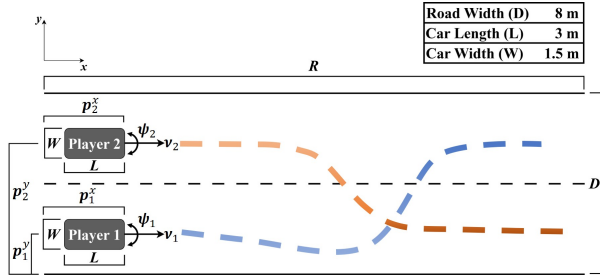


Figure 13: Lane change setup with two players.

where $\mu = 10^{-6}$, $\kappa = 100$, $\bar{p}_1^y = 6m$ for player 1 and $\bar{p}_2^y = 2m$ for player 2, $\bar{v} = 18m/s$, $\bar{\psi} = 0rad$, and $T = 4s$.

Data. In the case of supervised learning, we generate 1.45k ground truth trajectories by uniformly sampling initial states from the set $\mathcal{X}_{GT}^1 := [0, 3]m \times [1.25, 2.75]m \times [-\pi/180, \pi/180]rad \times [18, 25]m/s$ for player 1, and $\mathcal{X}_{GT}^2 := [0, 3]m \times [5.25, 6.75]m \times [-\pi/180, \pi/180]rad \times [18, 25]m/s$ for player 2, resulting in a total of 118.9k data points. For vanilla and value-hardening PIML, we uniformly sample 162k states from the set $\mathcal{X}_{HJ}^1 := [0, 95]m \times [0, 6]m \times [-0.15, 0.13]rad \times [17, 26]m/s$ for player 1, and $\mathcal{X}_{HJ}^2 := [0, 95]m \times [2, 8]m \times [-0.13, 0.15]rad \times [17, 26]m/s$ for player 2. In the case of hybrid learning, we generate 1k ground truth trajectories (82k data points) by uniformly sampling initial states from \mathcal{X}_{GT}^1 for player 1, and \mathcal{X}_{GT}^2 for player 2. Additionally, we sample 80k states uniformly from \mathcal{X}_{HJ}^1 for player 1, and \mathcal{X}_{HJ}^2 for player 2. For epigraphical learning, we initially gather a sample of 200k states from \mathcal{X}_{HJ} to ensure

adherence to the boundary condition. We set the range of the auxiliary state z_i as $[-9.5 \times 10^{-5}, 400]$. All other settings follow Case 1.

Training. In this experiment, we employ the Adam optimizer with a constant learning rate of 1×10^{-4} . For vanilla PIML, we initiate the pre-training phase with 10k iterations, utilizing 162k boundary states uniformly sampled. Subsequently, we continue with the training phase, performing 350k iterations. For value hardening, we set the training duration for each hardening step to 7.2k iterations, completing a total of 50 steps to ensure a fair comparison. All other settings remain consistent with those of Case 1.

Table VI: Safety performance w/ different activation functions under \mathcal{X}_{GT}

Test Domain	Activation Functions	Learning Method				
		HL	VH	EL	SL	PIML
\mathcal{X}_{GT}	tanh	0.00%	23.0%	46.2%	0.33%	30.2%
	relu	1.33%	40.3%	61.0%	0.00%	52.5%
	sine	0.50%	11.2%	48.5%	1.00%	17.3%

Results. We assess the safety performance on a test set comprising 600 ground truth collision-free trajectories. These trajectories are generated by sampling initial states from \mathcal{X}_{GT} . The results are summarized in Table VI, while the interaction distances between players are visualized in Fig. 15. Similar to Cases 1 and 2, the hybrid method demonstrates superior performance compared to the others. Similar to Case 2, value hardening fails to generalize effectively within a computational budget similar to hybrid learning. Fig. 14 shows interaction

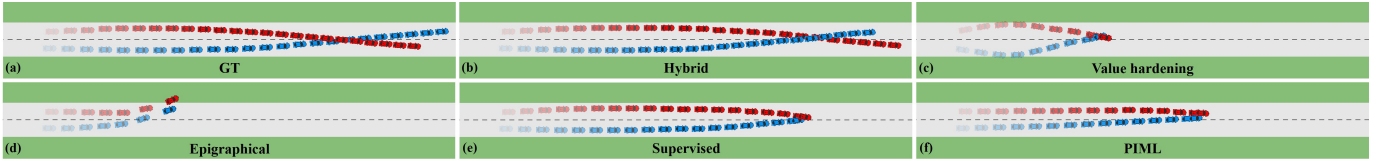


Figure 14: Double lane change visualization: (a): Ground truth safe trajectory. Transparency reduces along time. (b-e): Trajectories generated using hybrid, value hardening, epigraphical, supervised, and vanilla PIML models, respectively.

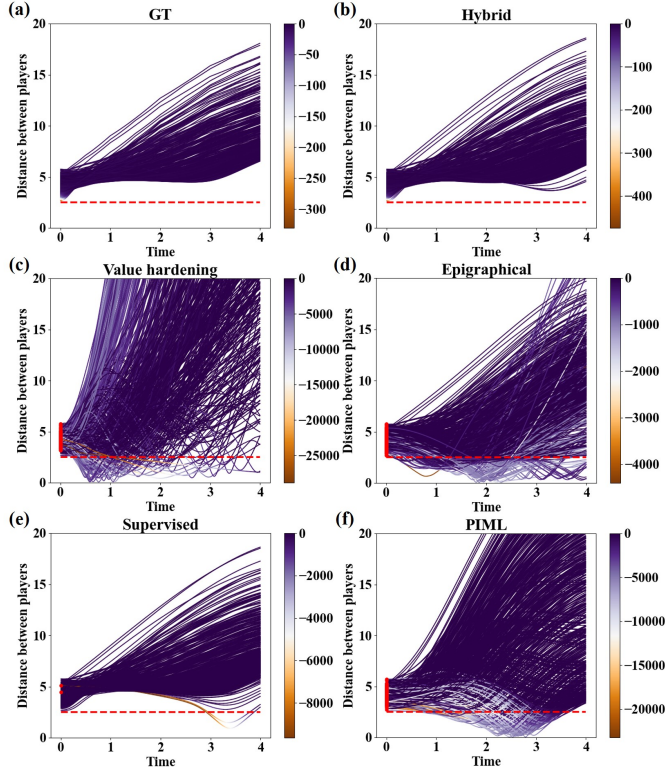


Figure 15: (a): Ground truth distance between players over time for \mathcal{X}_{GT} . (b-e): Distance between players over time using hybrid, value hardening, epigraphical, supervised, and vanilla PIML models under \mathcal{X}_{GT} , respectively. Red dashed line represents the threshold distance for collision.

trajectories starting from one particular initial state where the hybrid method achieves safe interaction while the others fail.

D. Case 4: two-drone collision avoidance

Experiment setup. In this experiment, we consider that the states of Player i consist of its location (p_i^x, p_i^y, p_i^z) , and speed (v_i^x, v_i^y, v_i^z) , denoted as $x_i := [p_i^x, p_i^y, p_i^z, v_i^x, v_i^y, v_i^z]^T$. We use the flight dynamics (in the near-hover regime, at zero yaw with respect to a global coordinate frame) described in [38]:

$$\begin{bmatrix} \dot{p}_i^x \\ \dot{p}_i^y \\ \dot{p}_i^z \\ \dot{v}_i^x \\ \dot{v}_i^y \\ \dot{v}_i^z \end{bmatrix} = \begin{bmatrix} v_i^x \\ v_i^y \\ v_i^z \\ g \tan(\theta_i) \\ -g \tan(\phi_i) \\ \tau_i - g \end{bmatrix}, \quad (33)$$

where the tracking control $u_i = (\theta_i, \phi_i, \tau_i)$ corresponds to roll, pitch and thrust. In this experiment, $\theta_i \in [-0.05, 0.05]rad$, $\phi_i \in [-0.05, 0.05]rad$, $\tau_i \in [7.81, 11.81]m/s^2$, and $g = 9.81m/s^2$. Note that we have assumed a zero yaw angle for the

quadrotor. The instantaneous loss considers the control effort and the collision penalty:

$$l_i(\mathbf{x}_i, \omega_i, u_i) = k_\theta \tan^2(\theta_i) + k_\phi \tan^2(\phi_i) + (\tau_i - g)^2 + b\sigma(\mathbf{x}_i, \eta), \quad (34)$$

where the penalty function is defined as

$$\sigma(\mathbf{x}_i, \eta) = (1 + \exp(\gamma(S - \eta)))^{-1},$$

$$S = \sqrt{((R_x - p_2^x) - p_1^x)^2 + ((R_y - p_2^y) - p_1^y)^2 + (p_2^z - p_1^z)^2}.$$

$b = 10^4$ and $\gamma = 5$. Additionally, the parameters $R_x = 5m$ and $R_y = 5m$ are used to transform the coordinate positions of the two players along the x - and y - axes, respectively. The values of $k_\theta = 100$ and $k_\phi = 100$ determine the trade-off between control effort for roll, pitch, and thrust. Furthermore, $\eta = 0.9m$ represents the collision threshold. The terminal loss is set to encourage players to move along their respective x and y directions, to return to $0m$ on the z axis, and to remain stationary when the simulation is complete:

$$g_i(x_i) = -\mu p_i^x(T) - \mu p_i^y(T) + (p_i^z(T) - \bar{p}_i^z)^2 + (v_i^x(T) - \bar{v}_i^x)^2 + (v_i^y(T) - \bar{v}_i^y)^2 + (v_i^z(T) - \bar{v}_i^z)^2. \quad (35)$$

where $\mu = 10^{-6}$, $\bar{p}_i^z = 0m$, $\bar{v}_i^x = \bar{v}_i^y = \bar{v}_i^z = 0m/s$, and $T = 4s$. In this case study, we only compare the generalization and safety performance between the hybrid and the supervised methods, and use vanilla PIML as a baseline. Value hardening and epigraphical learning are dropped since they lack scalability in higher-dimensional cases.

Data. In the case of supervised learning, we generate 1.25k ground truth trajectories by uniformly sampling initial states from the set $\mathcal{X}_{GT} := [0, 1]m \times [0, 1]m \times [-0.1, 0.1]m \times [2, 4]m/s \times [2, 4]m/s \times [0, 0.1]m/s$, resulting in a total of 102.5k data points. For vanilla PIML, we uniformly sample 162k states from the set $\mathcal{X}_{HJ} := [0, 15.5]m \times [0, 15.5]m \times [-1.8, 2]m \times [0.3, 4.5]m/s \times [0.3, 4.5]m/s \times [-1.8, 1.8]m/s$. In the case of hybrid learning, we generate 1k ground truth trajectories (82k data points) by uniformly sampling initial states from \mathcal{X}_{GT} . Additionally, we sample 80k states uniformly from \mathcal{X}_{HJ} .

Training. We use the Adam optimizer with a fixed learning rate of 1×10^{-4} . For vanilla PIML, we pre-train the networks for 100k iterations using 162k uniformly sampled boundary states and subsequently train them for an additional 400k iterations. The remaining settings for this experiment align with those used in Case 1.

Results. We assess the safety performance on a test set comprising 600 ground truth collision-free trajectories. These trajectories are generated by uniformly sampling initial states from \mathcal{X}_{GT} . The results are summarized in Table VII, while the

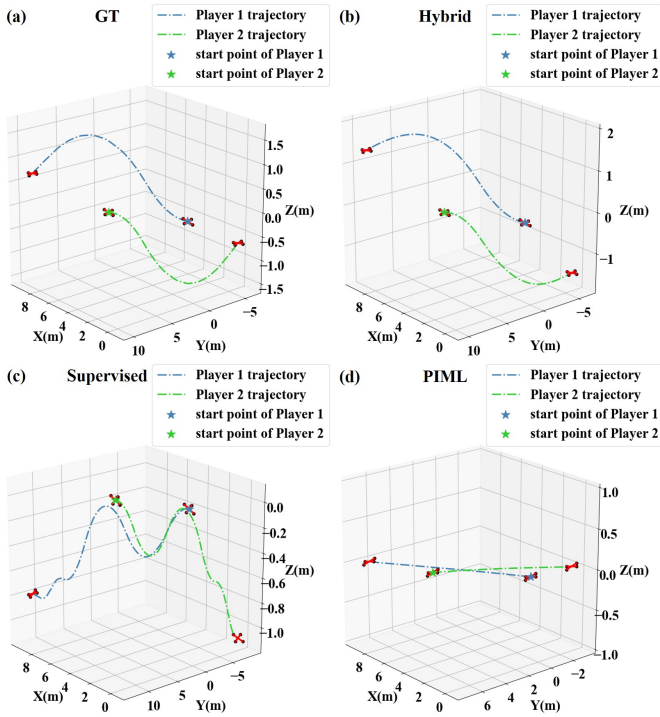


Figure 16: Two-drone collision avoidance visualization: (a): Ground truth safe trajectory. (b-d): Trajectories generated using hybrid, supervised, and vanilla PIML models, respectively.

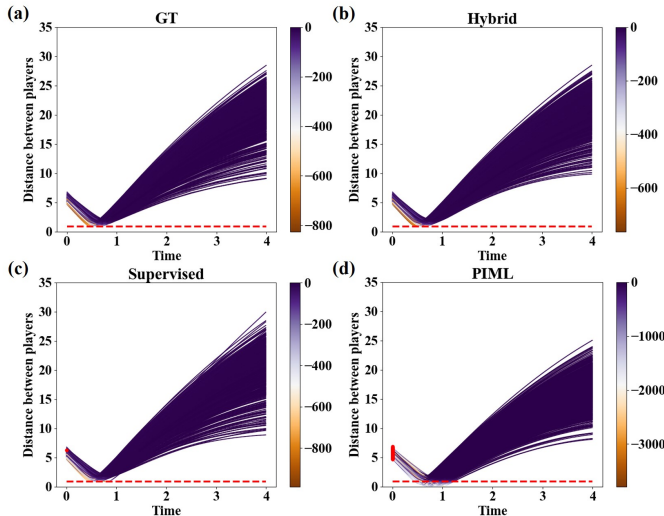


Figure 17: (a): Ground truth distance between players over time for \mathcal{X}_{GT} . (b-d): Distance between players over time using hybrid, supervised, and vanilla PIML models under \mathcal{X}_{GT} , respectively. Red dashed line represents the threshold distance for collision.

Table VII: Safety performance w/ different activation functions under \mathcal{X}_{GT}

Test Domain	Activation Functions	Learning Method		
		HL	SL	PIML
\mathcal{X}_{GT}	tanh	0.00%	0.17%	75.8%
	relu	34.0%	0.67%	76.2%
	sine	0.00%	0.17%	75.7%

interaction distances between players are visualized in Fig. 17. Similar to the first three cases, the hybrid learning method demonstrates superior performance compared to the other

methods. Fig. 16 visualizes the interaction trajectories starting from a particular initial state where the hybrid method achieves safe interaction, while the other baselines yield collisions and undesired trajectories.

V. CONCLUSION

We proposed a hybrid learning approach that combines the strengths of both supervised learning and vanilla PIML to approximate discontinuous value functions as solutions to two-player general-sum differential games. In particular, we have shown that our proposed method yields better generalization and safety performance than an array of baselines, including supervised learning, vanilla PIML, value hardening, and epigraphical learning, when using the same computational budget.

Several open questions arise from our investigation:

(1) Among all value approximation methods, some approximate the unsafe zone well but have poor safety performance when used for closed-loop control, e.g., the epigraphical method, while some others achieve good safety performance without accurately approximating the unsafe zone, e.g., the hybrid method. See results from Case 1 and Fig. 4. Considering that neither of these application-specific metrics, i.e., safety and the accuracy of approximating the unsafe zone, is directly used as the learning objective, the observation here prompts the following question: What learning algorithm can directly optimize for these application-specific metrics? To answer this question, we may need to first draw connection between PIML and reinforcement learning (RL). In the case where system dynamics is known and neural network is used for approximation, PIML and RL are similar in that i) both losses are based on Bellman backup, although usually in continuous and discrete time, respectively, and ii) both are Monte Carlo methods. The difference in sampling, however, is that while RL prioritizes on samples generated from a given initial state distribution, PIML approximates values across the entire space-time (which is necessary for safety). This connection may allow us to borrow existing analysis and techniques from RL to PIML, e.g., parallel training of value and policy (primal and dual) networks and importance sampling on experience replay.

(2) The epigraphical technique introduces an augmented state z to facilitate the learning of a smooth value function. From our experiments, however, this technique requires a significantly higher computational cost to achieve reasonable value approximation as shown in Table I, even with careful design of the network architecture (i.e., the exploitation of the structure of the augmented value). There is a lack of analytical understanding of how the augmented state affects the computational complexity of PIML.

VI. APPENDIX

A. Proof of Lemma 1 (Following the proofs in [47] to prove Lemma 1)

Proof. (i) $\vartheta_i(\mathbf{x}_i, t) - z_i \leq 0$ implies that there exists $\alpha_i \in \mathcal{A}$ such that

$$\int_t^T l_i(x_s^{\mathbf{x}_i, t, \alpha_i}, \alpha_i(x_s^{\mathbf{x}_i, t, \alpha_i, \alpha_{-i}})) ds + g_i(x_T^{\mathbf{x}_i, t, \alpha_i}) - z_i \leq 0, \quad (36)$$

and $c_i(\mathbf{x}_s^{\mathbf{x}_i, t, \alpha_i, \alpha^{-i}}) \leq 0$ for $s \in [t, T]$. Thus, there exists α_i such that $V_i(\mathbf{x}_i, z_i, t) \leq 0$.

(ii) $V_i(\mathbf{x}_i, z_i, t) \leq 0$ and $c_i(\mathbf{x}_s^{\mathbf{x}_i, t, \alpha_i, \alpha^{-i}}) \leq 0$ implies that there exists $\alpha_i \in \mathcal{A}$ such that

$$\int_t^T l_i(x_s^{\mathbf{x}_i, t, \alpha_i}, \alpha_i(\mathbf{x}_s^{\mathbf{x}_i, t, \alpha_i, \alpha^{-i}})) ds + g_i(x_T^{\mathbf{x}_i, t, \alpha_i}) - z_i \leq 0. \quad (37)$$

which concludes $\vartheta_i(\mathbf{x}_i, t) - z_i \leq 0$. \square

B. Proof of Lemma 2 (Following the proofs in [47], [53] to prove Lemma 2)

Proof. For any policy α_i and a small step $h > 0$, we can use Eq. (7) to derive the following relation (α_{-i}^* represents equilibrium policy for the fellow player of Player i).

$$\begin{aligned} V_i(\mathbf{x}_i, z_i, t) &= \min_{\alpha_i \in \mathcal{A}} \max \left\{ \max_{s \in [t, T]} c_i(\mathbf{x}_s^{\mathbf{x}_i, t, \alpha_i, \alpha_{-i}^*}), \right. \\ &\quad \left. g_i(x_T^{\mathbf{x}_i, t, \alpha_i}) - z_i(T) \right\}, \\ &= \max \left\{ \max_{s \in [t, t+h]} c_i(\mathbf{x}_s^{\mathbf{x}_i, t, \alpha_i, \alpha_{-i}^*}), \right. \\ &\quad \max \left\{ \max_{s \in [t+h, T]} c_i(\mathbf{x}_s^{\mathbf{x}_i, t, \alpha_i, \alpha_{-i}^*}), \right. \\ &\quad \left. \left. g_i(x_T^{\mathbf{x}_i, t, \alpha_i}) - z_i(T) \right\} \right\}. \end{aligned}$$

There exists two different policies $\alpha_{i1}, \alpha_{i2} \in \mathcal{A}$ such that

$$\alpha_i = \begin{cases} \alpha_{i1}(s), & s \in [t, t+h], \\ \alpha_{i2}(s), & s \in (t+h, T]. \end{cases}$$

Then we have

$$\begin{aligned} V_i(\mathbf{x}_i, z_i, t) &= \min_{\alpha_{i1} \in \mathcal{A}, \alpha_{i2} \in \mathcal{A}} \max \left\{ \max_{s \in [t, t+h]} c_i(\mathbf{x}_s^{\mathbf{x}_i, t, \alpha_i, \alpha_{-i}^*}), \right. \\ &\quad \max \left\{ \max_{s \in [t+h, T]} c_i(\mathbf{x}_s^{\mathbf{x}_i, t, \alpha_i, \alpha_{-i}^*}) \right. \\ &\quad \left. \left. g_i(x_T^{\mathbf{x}_i, t, \alpha_i}) - z_i(T) \right\} \right\}, \\ &= \min_{\alpha_{i1} \in \mathcal{A}} \max \left\{ \max_{s \in [t, t+h]} c_i(\mathbf{x}_s^{\mathbf{x}_i, t, \alpha_i, \alpha_{-i}^*}), \right. \\ &\quad \min_{\alpha_{i2} \in \mathcal{A}} \max \left\{ \max_{s \in [t+h, T]} c_i(\mathbf{x}_s^{\mathbf{x}_i, t, \alpha_i, \alpha_{-i}^*}), \right. \\ &\quad \left. \left. g_i(x_T^{\mathbf{x}_i, t, \alpha_i}) - z_i(T) \right\} \right\}, \\ &= \min_{\alpha_{i1} \in \mathcal{A}} \max \left\{ \max_{s \in [t, t+h]} c_i(\mathbf{x}_s^{\mathbf{x}_i, t, \alpha_i, \alpha_{-i}^*}), \right. \\ &\quad \left. V_i(\mathbf{x}_i(t+h), z_i(t+h), t+h) \right\}, \\ &= \min_{\alpha_i \in \mathcal{A}} \max \left\{ \max_{s \in [t, t+h]} c_i(\mathbf{x}_s^{\mathbf{x}_i, t, \alpha_i, \alpha_{-i}^*}), \right. \\ &\quad \left. V_i(\mathbf{x}_i(t+h), z_i(t+h), t+h) \right\}. \end{aligned}$$

\square

C. Proof of Theorem 1 (Following the proofs in [47], [53] to prove Theorem 1)

Proof. (i) When $t = T$, V_i is easily satisfied based on definition

$$\begin{aligned} V_i(\mathbf{x}_i, z_i, T) &= \max \left\{ c_i(\mathbf{x}_T^{\mathbf{x}_i, T, \alpha_i, \alpha_{-i}^*}), g_i(x_T^{\mathbf{x}_i, T, \alpha_i}) - z_i(T) \right\} \\ &\quad \max \{c_i(\mathbf{x}_i(T)), g_i(T) - z_i(T)\} \end{aligned} \quad (38)$$

(ii) Let $W_i \in C^\infty(\mathcal{X} \times \mathbb{R} \times [0, T])$, and assume that $V_i - W_i$ has local maximum at $(\mathbf{x}_i(t_0), z_i(t_0), t_0) \in \mathcal{X} \times \mathbb{R} \times [0, T]$ and $(V_i - W_i)(\mathbf{x}_i(t_0), z_i(t_0), t_0) = 0$, we need to prove

$$\begin{aligned} &\max \left\{ c_i(\mathbf{x}_{t_0}^{\mathbf{x}_i, t_0, \alpha_i, \alpha_{-i}^*}) - W_i(\mathbf{x}_i(t_0), z_i(t_0), t_0), \right. \\ &\quad \nabla_t W_i(\mathbf{x}_i(t_0), z_i(t_0), t_0) - \mathcal{H}_i(t_0, \mathbf{x}_i(t_0), z_i(t_0), \\ &\quad \nabla_{\mathbf{x}_i} W_i(\mathbf{x}_i(t_0), z_i(t_0), t_0), \nabla_{z_i} W_i(\mathbf{x}_i(t_0), z_i(t_0), t_0)) \left. \right\} \\ &\quad \geq 0. \end{aligned} \quad (39)$$

Suppose not. Then there exists $\xi > 0$ and $\tilde{\alpha}_i \in \mathcal{A}$ such that

$$\begin{aligned} &c_i(\mathbf{x}_s^{\mathbf{x}_i, t, \tilde{\alpha}_i, \alpha_{-i}^*}) - W_i(\mathbf{x}_i(t_0), z_i(t_0), t_0) \leq -\xi, \\ &\nabla_t W_i(\mathbf{x}_i, z_i, t) + \nabla_{\mathbf{x}_i} W_i(\mathbf{x}_i, z_i, t) \cdot \mathbf{f}_i(\mathbf{x}_i, \tilde{\alpha}_i, \alpha_{-i}^*) \\ &\quad - \nabla_{z_i} W_i(\mathbf{x}_i, z_i, t) \cdot l_i \left(x_s^{\mathbf{x}_i, t, \tilde{\alpha}_i}, \tilde{\alpha}_i \left(\mathbf{x}_s^{\mathbf{x}_i, t, \tilde{\alpha}_i, \alpha_{-i}^*} \right) \right) \leq -\xi. \end{aligned} \quad (40)$$

for all points (\mathbf{x}_i, z_i, t) sufficiently close to $(\mathbf{x}_i(t_0), z_i(t_0), t_0)$: there exists small enough $h_1 > 0$ such that $\|\mathbf{x}_i - \mathbf{x}_i(t_0)\| + |z_i - z_i(t_0)| + |t - t_0| < h_1$. According to Assumptions in Section III-B, choose a small h such that $\|\mathbf{x}_i - \mathbf{x}_i(t_0)\| + |z_i - z_i(t_0)| < h_1 - h$ for $s \in [t_0, t_0 + h]$, then

$$\begin{aligned} &c_i(\mathbf{x}_s^{\mathbf{x}_i, t, \tilde{\alpha}_i, \alpha_{-i}^*}) - W_i(\mathbf{x}_i(t_0), z_i(t_0), t_0) \leq -\xi, \\ &\nabla_t W_i(\mathbf{x}_i, z_i, s) + \nabla_{\mathbf{x}_i} W_i(\mathbf{x}_i, z_i, s) \cdot \mathbf{f}_i(\mathbf{x}_i, \tilde{\alpha}_i, \alpha_{-i}^*) \\ &\quad - \nabla_{z_i} W_i(\mathbf{x}_i, z_i, s) \cdot l_i \left(x_s^{\mathbf{x}_i, t, \tilde{\alpha}_i}, \tilde{\alpha}_i \left(\mathbf{x}_s^{\mathbf{x}_i, t, \tilde{\alpha}_i, \alpha_{-i}^*} \right) \right) \leq -\xi. \end{aligned} \quad (41)$$

According to the condition that $V_i - W_i$ has a local maximum at $(\mathbf{x}(t_0), z_i(t_0), t_0)$, then

$$\begin{aligned} &V_i(\mathbf{x}_i(t_0 + h), z_i(t_0 + h), t_0 + h) \\ &\quad - W_i(\mathbf{x}_i(t_0 + h), z_i(t_0 + h), t_0 + h) \\ &\leq V_i(\mathbf{x}_i(t_0), z_i(t_0), t_0) - W_i(\mathbf{x}(t_0), z_i(t_0), t_0) \\ &\Rightarrow V_i(\mathbf{x}_i(t_0 + h), z_i(t_0 + h), t_0 + h) - V_i(\mathbf{x}_i(t_0), z_i(t_0), t_0) \\ &\leq W_i(\mathbf{x}_i(t_0 + h), z_i(t_0 + h), t_0 + h) - W_i(\mathbf{x}_i(t_0), z_i(t_0), t_0) \\ &\Rightarrow V_i(\mathbf{x}_i(t_0 + h), z_i(t_0 + h), t_0 + h) - V_i(\mathbf{x}_i(t_0), z_i(t_0), t_0) \\ &\leq \int_{t_0}^{t_0+h} \frac{dW_i}{dt} ds \\ &\Rightarrow V_i(\mathbf{x}_i(t_0 + h), z_i(t_0 + h), t_0 + h) - V_i(\mathbf{x}_i(t_0), z_i(t_0), t_0) \\ &\leq \int_{t_0}^{t_0+h} \left\{ \nabla_t W_i(\mathbf{x}_i, z_i, s) + \nabla_{\mathbf{x}_i} W_i(\mathbf{x}_i, z_i, s) \cdot \mathbf{f}_i \right. \\ &\quad \left. - \nabla_{z_i} W_i(\mathbf{x}_i, z_i, s) \cdot l_i \right\} ds \leq -\xi h \end{aligned} \quad (42)$$

\square

Lemma 2 says that

$$V_i(\mathbf{x}_i(t_0), z_i(t_0), t_0) = \min_{u_i \in \mathcal{U}_i} \max \left\{ \max_{s \in [t_0, t_0+h]} c_i(\mathbf{x}_i(s)), \right. \\ \left. V_i(\mathbf{x}_i(t_0+h), z_i(t_0+h), t_0+h) \right\}, \quad (43)$$

Eq. (43) subtracts $W_i(\mathbf{x}_i(t_0), z_i(t_0), t_0)$ on the both side and combines Eq. (41) and (42)

$$0 = (V_i - W_i)(\mathbf{x}_i(t_0), z_i(t_0), t_0) \\ = \min_{u_i \in \mathcal{U}_i} \max \{-\xi, -\xi h\} < 0, \quad (44)$$

which is a contradiction. Thus, we prove that

$$\max \left\{ c_i(\mathbf{x}_{t_0}^{\mathbf{x}_i, t, \alpha_i, \alpha_{-i}^*}) - W_i(\mathbf{x}_i(t_0), z_i(t_0), t_0), \right. \\ \nabla_t W_i(\mathbf{x}_i(t_0), z_i(t_0), t_0) - \mathcal{H}_i(t_0, \mathbf{x}_i(t_0), z_i(t_0)), \\ \nabla_{\mathbf{x}_i} W_i(\mathbf{x}_i(t_0), z_i(t_0), t_0), \nabla_{z_i} W_i(\mathbf{x}_i(t_0), z_i(t_0), t_0)) \left. \right\} \\ \geq 0. \quad (45)$$

(iii) Let $W_i \in C^\infty(\mathcal{X} \times \mathbb{R} \times [0, T])$, and assume that $V_i - W_i$ has local minimum at $(\mathbf{x}_i(t_0), z_i(t_0), t_0) \in \mathcal{X} \times \mathbb{R} \times [0, T]$ and $(V_i - W_i)(\mathbf{x}_i(t_0), z_i(t_0), t_0) = 0$, we need to prove

$$\max \left\{ c_i(\mathbf{x}_{t_0}^{\mathbf{x}_i, t, \alpha_i, \alpha_{-i}^*}) - W_i(\mathbf{x}_i(t_0), z_i(t_0), t_0), \right. \\ \nabla_t W_i(\mathbf{x}_i(t_0), z_i(t_0), t_0) - \mathcal{H}_i(t_0, \mathbf{x}_i(t_0), z_i(t_0)), \\ \nabla_{\mathbf{x}_i} W_i(\mathbf{x}_i(t_0), z_i(t_0), t_0), \nabla_{z_i} W_i(\mathbf{x}_i(t_0), z_i(t_0), t_0)) \left. \right\} \\ \leq 0. \quad (46)$$

The definition of V_i says that

$$V_i(\mathbf{x}_i(t_0), z_i(t_0), t_0) = \max \left\{ \max_{s \in [t_0, T]} c_i(\mathbf{x}_s^{\mathbf{x}_i, t, \alpha_i, \alpha_{-i}^*}), \right. \\ \left. g_i(x_T^{\mathbf{x}_i, t, \alpha_i}) - z_i(T) \right\}, \\ \geq \max \left\{ c_i(\mathbf{x}_{t_0}^{\mathbf{x}_i, t, \alpha_i, \alpha_{-i}^*}), \right. \\ \left. g_i(x_T^{\mathbf{x}_i, t, \alpha_i}) - z_i(T) \right\}. \quad (47)$$

for all $\alpha_i \in \mathcal{A}(t_0)$. Eq. (47) subtracts $W_i(\mathbf{x}_i(t_0), z_i(t_0), t_0)$ on both sides and has that

$$0 = (V_i - W_i)(\mathbf{x}_i(t_0), z_i(t_0), t_0) \geq \max \{ c_i(\mathbf{x}_{t_0}^{\mathbf{x}_i, t, \alpha_i, \alpha_{-i}^*}) - \\ W_i(\mathbf{x}_i(t_0), z_i(t_0), t_0), g_i(x_T^{\mathbf{x}_i, t, \alpha_i}) - z_i(T) - \\ W_i(\mathbf{x}_i(t_0), z_i(t_0), t_0) \}. \quad (48)$$

Then we must prove the following inequality

$$\nabla_t W_i(\mathbf{x}_i(t_0), z_i(t_0), t_0) - \mathcal{H}_i(t_0, \mathbf{x}_i(t_0), z_i(t_0)), \\ \nabla_{\mathbf{x}_i} W_i(\mathbf{x}_i(t_0), z_i(t_0), t_0), \nabla_{z_i} W_i(\mathbf{x}_i(t_0), z_i(t_0), t_0)) \leq 0, \quad (49)$$

Suppose not. Then there exists $\xi > 0$ such that

$$\nabla_t W_i(\mathbf{x}_i, z_i, t) - \max_{u_i \in \mathcal{U}_i} \left[-\nabla_{\mathbf{x}_i} W_i(\mathbf{x}_i, z_i, t) \cdot \mathbf{f}_i \right. \\ \left. + \nabla_{z_i} W_i(\mathbf{x}_i, z_i, t) \cdot l_i \right] \geq \xi, \quad (50)$$

for all points (\mathbf{x}_i, z_i, t) sufficiently close to $(\mathbf{x}_i(t_0), z_i(t_0), t_0)$: there exists small enough $h_1 > 0$ such that $\|\mathbf{x}_i - \mathbf{x}_i(t_0)\| + |z_i - z_i(t_0)| + |t - t_0| < h_1$. For any $\alpha_i \in \mathcal{A}$, where

$$\alpha_i \in \arg \max_{\alpha_i \in \mathcal{A}} -\nabla_{\mathbf{x}_i} W_i(\mathbf{x}_i, z_i, s) \cdot \mathbf{f}_i(\mathbf{x}_i, \alpha_i, \alpha_{-i}^*) \\ + \nabla_{z_i} W_i(\mathbf{x}_i, z_i, s) \cdot l_i \left(x_s^{\mathbf{x}_i, t, \alpha_i}, \alpha_i \left(\mathbf{x}_s^{\mathbf{x}_i, t, \alpha_i, \alpha_{-i}^*} \right) \right), \quad (51)$$

According to Assumptions in Section III-B, choose a small h such that $\|\mathbf{x}_i - \mathbf{x}_i(t_0)\| + |z_i - z_i(t_0)| < h_1 - h$ for $s \in [t_0, t_0 + h]$, then

$$\nabla_t W_i(\mathbf{x}_i, z_i, s) + \nabla_{\mathbf{x}_i} W_i(\mathbf{x}_i, z_i, s) \cdot \mathbf{f}_i(\mathbf{x}_i, \alpha_i, \alpha_{-i}^*) \\ - \nabla_{z_i} W_i(\mathbf{x}_i, z_i, s) \cdot l_i \left(x_s^{\mathbf{x}_i, t, \alpha_i}, \alpha_i \left(\mathbf{x}_s^{\mathbf{x}_i, t, \alpha_i, \alpha_{-i}^*} \right) \right) \geq \xi, \quad (52)$$

for all $s \in [t_0, t_0 + h]$. We integrate Eq. (52) over $s \in [t_0, t_0 + h]$ to get

$$W_i(\mathbf{x}_i(t_0+h), z_i(t_0+h), t_0+h) \\ - W_i(\mathbf{x}_i(t_0), z_i(t_0), t_0) \geq \xi h, \quad (53)$$

We have the following relation because Eq. (53) holds for all $u_i \in \mathcal{U}_i$

$$\min_{u_i \in \mathcal{U}_i} W_i(\mathbf{x}_i(t_0+h), z_i(t_0+h), t_0+h) \\ - W_i(\mathbf{x}_i(t_0), z_i(t_0), t_0) \geq \xi h, \quad (54)$$

According to the condition that $V_i - W_i$ has a local minimum at $(\mathbf{x}_i(t_0), z_i(t_0), t_0)$, then

$$\min_{u_i \in \mathcal{U}_i} V_i(\mathbf{x}_i(t_0+h), z_i(t_0+h), t_0+h) \\ - V_i(\mathbf{x}_i(t_0), z_i(t_0), t_0) \\ \geq \min_{u_i \in \mathcal{U}_i} W_i(\mathbf{x}_i(t_0+h), z_i(t_0+h), t_0+h) \\ - W_i(\mathbf{x}_i(t_0), z_i(t_0), t_0) \\ \geq \xi h \\ \Rightarrow \min_{u_i \in \mathcal{U}_i} V_i(\mathbf{x}_i(t_0+h), z_i(t_0+h), t_0+h) \\ > V_i(\mathbf{x}_i(t_0), z_i(t_0), t_0) \quad (55)$$

However, Lemma 2 says that

$$\min_{u_i \in \mathcal{U}_i} V_i(\mathbf{x}_i(t_0+h), z_i(t_0+h), t_0+h) \leq V_i(\mathbf{x}_i(t_0), z_i(t_0), t_0), \quad (56)$$

which is a contradiction. Thus, we prove that

$$\max \left\{ c_i(\mathbf{x}_{t_0}^{\mathbf{x}_i, t, \alpha_i, \alpha_{-i}^*}) - W_i(\mathbf{x}_i(t_0), z_i(t_0), t_0), \right. \\ \nabla_t W_i(\mathbf{x}_i(t_0), z_i(t_0), t_0) - \mathcal{H}_i(t_0, \mathbf{x}_i(t_0), z_i(t_0)), \\ \nabla_{\mathbf{x}_i} W_i(\mathbf{x}_i(t_0), z_i(t_0), t_0), \nabla_{z_i} W_i(\mathbf{x}_i(t_0), z_i(t_0), t_0)) \left. \right\} \\ \leq 0. \quad (57)$$

Hence, we prove that $V_i(\mathbf{x}_i, z_i, t)$ is the unique viscosity solution. \square

ACKNOWLEDGMENTS

This work was in part supported by NSF CMMI-1925403 and NSF CNS-2101052. The views and conclusions contained in this document are those of the authors and should not be interpreted as representing the official policies, either expressed or implied, of the National Science Foundation or the U.S. Government.

REFERENCES

- [1] F. Duarte and C. Ratti, "The impact of autonomous vehicles on cities: A review," *Journal of Urban Technology*, vol. 25, no. 4, pp. 3–18, 2018.
- [2] B. S. Peters, P. R. Armijo, C. Krause, S. A. Choudhury, and D. Oleynikov, "Review of emerging surgical robotic technology," *Surgical endoscopy*, vol. 32, pp. 1636–1655, 2018.
- [3] R. R. Murphy, "Human-robot interaction in rescue robotics," *IEEE Transactions on Systems, Man, and Cybernetics, Part C (Applications and Reviews)*, vol. 34, no. 2, pp. 138–153, 2004.
- [4] K. Leung, E. Schmerling, M. Zhang, M. Chen, J. Talbot, J. C. Gerdes, and M. Pavone, "On infusing reachability-based safety assurance within planning frameworks for human-robot vehicle interactions," *The International Journal of Robotics Research*, vol. 39, no. 10-11, pp. 1326–1345, 2020.
- [5] N. Gammoudi and H. Zidani, "A differential game control problem with state constraints," *Mathematical Control and Related Fields*, vol. 13, no. 2, pp. 554–582, 2023.
- [6] R. Bellman and R. E. Kalaba, *Dynamic programming and modern control theory*. Citeseer, 1965, vol. 81.
- [7] E. Weinan, J. Han, and A. Jentzen, "Algorithms for solving high dimensional PDEs: from nonlinear Monte Carlo to machine learning," *Nonlinearity*, vol. 35, no. 1, p. 278, 2021.
- [8] Y. Shin, J. Darbon, and G. E. Karniadakis, "On the convergence of physics informed neural networks for linear second-order elliptic and parabolic type PDEs," *arXiv preprint arXiv:2004.01806*, 2020.
- [9] K. Ito, C. Reisinger, and Y. Zhang, "A neural network-based policy iteration algorithm with global H^2 -superlinear convergence for stochastic games on domains," *Foundations of Computational Mathematics*, vol. 21, no. 2, pp. 331–374, 2021.
- [10] O. L. Mangasarian, "Sufficient conditions for the optimal control of nonlinear systems," *SIAM Journal on control*, vol. 4, no. 1, pp. 139–152, 1966.
- [11] Y. Bengio, J. Louradour, R. Collobert, and J. Weston, "Curriculum learning," in *Proceedings of the 26th annual international conference on machine learning*, 2009, pp. 41–48.
- [12] A. Altarovi, O. Bokanowski, and H. Zidani, "A general Hamilton-Jacobi framework for non-linear state-constrained control problems," *ESAIM: Control, Optimisation and Calculus of Variations*, vol. 19, no. 2, pp. 337–357, 2013.
- [13] M. Raissi, P. Perdikaris, and G. E. Karniadakis, "Physics-informed neural networks: A deep learning framework for solving forward and inverse problems involving nonlinear partial differential equations," *Journal of Computational physics*, vol. 378, pp. 686–707, 2019.
- [14] M. Raissi, Z. Wang, M. S. Triantafyllou, and G. E. Karniadakis, "Deep learning of vortex-induced vibrations," *Journal of Fluid Mechanics*, vol. 861, pp. 119–137, 2019.
- [15] D. Hendrycks and K. Gimpel, "Gaussian error linear units (GELUs)," *arXiv preprint arXiv:1606.08415*, 2016.
- [16] S. Bansal and C. J. Tomlin, "DeepReach: A deep learning approach to high-dimensional reachability," in *2021 IEEE International Conference on Robotics and Automation (ICRA)*. IEEE, 2021, pp. 1817–1824.
- [17] A. D. Jagtap, K. Kawaguchi, and G. E. Karniadakis, "Adaptive activation functions accelerate convergence in deep and physics-informed neural networks," *Journal of Computational Physics*, vol. 404, p. 109136, 2020.
- [18] L. Zhang, M. Ghimire, W. Zhang, Z. Xu, and Y. Ren, "Approximating discontinuous Nash equilibrium values of two-player general-sum differential games," in *2023 IEEE International Conference on Robotics and Automation (ICRA)*. IEEE, 2023, pp. 3022–3028.
- [19] M. G. Crandall and P.-L. Lions, "Viscosity solutions of Hamilton-Jacobi equations," *Transactions of the American mathematical society*, vol. 277, no. 1, pp. 1–42, 1983.
- [20] S. Osher and C.-W. Shu, "High-order essentially nonoscillatory schemes for Hamilton-Jacobi equations," *SIAM Journal on numerical analysis*, vol. 28, no. 4, pp. 907–922, 1991.
- [21] S. Osher, R. Fedkiw, and K. Piechor, "Level set methods and dynamic implicit surfaces," *Appl. Mech. Rev.*, vol. 57, no. 3, pp. B15–B15, 2004.
- [22] I. M. Mitchell and J. A. Templeton, "A toolbox of Hamilton-Jacobi solvers for analysis of nondeterministic continuous and hybrid systems," in *Hybrid Systems: Computation and Control: 8th International Workshop, HSCC 2005, Zurich, Switzerland, March 9-11, 2005. Proceedings 8*. Springer, 2005, pp. 480–494.
- [23] I. M. Mitchell and C. J. Tomlin, "Overapproximating reachable sets by Hamilton-Jacobi projections," *Journal of Scientific Computing*, vol. 19, no. 1, pp. 323–346, 2003.
- [24] J. Han and J. Long, "Convergence of the deep BSDE method for coupled FBSDEs," *Probability, Uncertainty and Quantitative Risk*, vol. 5, no. 1, pp. 1–33, 2020.
- [25] J. Han, A. Jentzen, and W. E. "Solving high-dimensional partial differential equations using deep learning," *Proceedings of the National Academy of Sciences*, vol. 115, no. 34, pp. 8505–8510, 2018.
- [26] T. Nakamura-Zimmerer, Q. Gong, and W. Kang, "Adaptive deep learning for high-dimensional Hamilton-Jacobi-Bellman equations," *SIAM Journal on Scientific Computing*, vol. 43, no. 2, pp. A1221–A1247, 2021.
- [27] D. Fridovich-Keil, E. Ratner, L. Peters, A. D. Dragan, and C. J. Tomlin, "Efficient iterative linear-quadratic approximations for nonlinear multi-player general-sum differential games," in *2020 IEEE international conference on robotics and automation (ICRA)*. IEEE, 2020, pp. 1475–1481.
- [28] J. N. Foerster, R. Y. Chen, M. Al-Shedivat, S. Whiteson, P. Abbeel, and I. Mordatch, "Learning with opponent-learning awareness," *arXiv:1709.04326 [cs]*, Sep. 2017, arXiv: 1709.04326.
- [29] D. Sadigh, N. Landolfi, S. S. Sastry, S. A. Seshia, and A. D. Dragan, "Planning for cars that coordinate with people: leveraging effects on human actions for planning and active information gathering over human internal state," *Autonomous Robots*, vol. 42, no. 7, pp. 1405–1426, Oct. 2018.
- [30] M. Kwon, E. Biyik, A. Talati, K. Bhasin, D. P. Losey, and D. Sadigh, "When humans aren't optimal: Robots that collaborate with risk-aware humans," in *Proceedings of the 2020 ACM/IEEE International Conference on Human-Robot Interaction*, 2020, pp. 43–52.
- [31] W. Schwarting, A. Pierson, J. Alonso-Mora, S. Karaman, and D. Rus, "Social behavior for autonomous vehicles," *Proceedings of the National Academy of Sciences*, vol. 116, no. 50, pp. 24 972–24 978, 2019.
- [32] Z. Zahedi, A. Khayatian, M. M. Arefi, and S. Yin, "Seeking Nash equilibrium in non-cooperative differential games," *Journal of Vibration and Control*, p. 10775463221122120, 2022.
- [33] J. Li, Z. Xiao, J. Fan, T. Chai, and F. L. Lewis, "Off-policy Q-learning: Solving Nash equilibrium of multi-player games with network-induced delay and unmeasured state," *Automatica*, vol. 136, p. 110076, 2022.
- [34] S. Nikolaidis, D. Hsu, and S. Srinivasa, "Human-robot mutual adaptation in collaborative tasks: Models and experiments," *The International Journal of Robotics Research*, vol. 36, no. 5-7, pp. 618–634, 2017.
- [35] L. Sun, W. Zhan, and M. Tomizuka, "Probabilistic prediction of interactive driving behavior via hierarchical inverse reinforcement learning," in *2018 21st International Conference on Intelligent Transportation Systems (ITSC)*. IEEE, 2018, pp. 2111–2117.
- [36] C. Peng and M. Tomizuka, "Bayesian persuasive driving," in *2019 American Control Conference (ACC)*. IEEE, 2019, pp. 723–729.
- [37] Y. Wang, Y. Ren, S. Elliott, and W. Zhang, "Enabling courteous vehicle interactions through game-based and dynamics-aware intent inference," *IEEE Transactions on Intelligent Vehicles*, vol. 5, no. 2, pp. 217–228, 2019.
- [38] D. Fridovich-Keil, A. Bajcsy, J. F. Fisac, S. L. Herbert, S. Wang, A. D. Dragan, and C. J. Tomlin, "Confidence-aware motion prediction for real-time collision avoidance," *The International Journal of Robotics Research*, vol. 39, no. 2-3, pp. 250–265, 2020.
- [39] Y. Chen, L. Zhang, T. Merry, S. Amatya, W. Zhang, and Y. Ren, "When shall i be empathetic? the utility of empathetic parameter estimation in multi-agent interactions," in *2021 IEEE International Conference on Robotics and Automation (ICRA)*. IEEE, 2021, pp. 2761–2767.
- [40] R. J. Aumann, M. Maschler, and R. E. Stearns, *Repeated games with incomplete information*. MIT press, 1995.
- [41] P. Cardaliaguet, "Differential games with asymmetric information," *SIAM journal on Control and Optimization*, vol. 46, no. 3, pp. 816–838, 2007.
- [42] Cardaliaguet, Pierre, "Numerical approximation and optimal strategies for differential games with lack of information on one side," *Advances in Dynamic Games and Their Applications: Analytical and Numerical Developments*, pp. 1–18, 2009.
- [43] P. Cardaliaguet and C. Rainer, "Games with incomplete information in continuous time and for continuous types," *Dynamic Games and Applications*, vol. 2, no. 2, pp. 206–227, 2012.
- [44] A. W. Starr and Y.-C. Ho, "Nonzero-sum differential games," *Journal of optimization theory and applications*, vol. 3, no. 3, pp. 184–206, 1969.
- [45] E. Cristiani and P. Martinon, "Initialization of the shooting method via the Hamilton-Jacobi-Bellman approach," *Journal of Optimization Theory and Applications*, vol. 146, no. 2, pp. 321–346, 2010.
- [46] O. Fuks and H. A. Tchelepi, "Limitations of physics informed machine learning for nonlinear two-phase transport in porous media," *Journal of Machine Learning for Modeling and Computing*, vol. 1, no. 1, 2020.

- [47] D. Lee, "Safety-guaranteed autonomy under uncertainty," Ph.D. dissertation, UC Berkeley, 2022.
- [48] A. Kumar, A. Zhou, G. Tucker, and S. Levine, "Conservative Q-learning for offline Reinforcement Learning," *Advances in Neural Information Processing Systems*, vol. 33, pp. 1179–1191, 2020.
- [49] P. Petersen and F. Voigtlaender, "Optimal approximation of piecewise smooth functions using deep ReLU neural networks," *Neural Networks*, vol. 108, pp. 296–330, 2018.
- [50] V. Sitzmann, J. Martel, A. Bergman, D. Lindell, and G. Wetzstein, "Implicit neural representations with periodic activation functions," *Advances in Neural Information Processing Systems*, vol. 33, pp. 7462–7473, 2020.
- [51] J. C. Harsanyi, "Games with incomplete information played by "Bayesian" players, I–III Part I. The basic model," *Management science*, vol. 14, no. 3, pp. 159–182, 1967.
- [52] Z.-Q. J. Xu, Y. Zhang, T. Luo, Y. Xiao, and Z. Ma, "Frequency principle: Fourier analysis sheds light on deep neural networks," *arXiv preprint arXiv:1901.06523*, 2019.
- [53] L. C. Evans, *Partial differential equations*. American Mathematical Society, 2022, vol. 19.

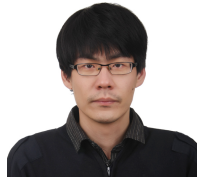


VII. BIOGRAPHY SECTION

Lei Zhang received his B.Eng. degree in process equipment and control engineering and M.Sci. degree in material engineering from Xi'an Jiaotong University, China, in 2010 and 2012, respectively. He is a Ph.D. candidate and research assistant in Design Informatics Lab, Arizona State University. His research interests include Machine Learning, Optimization, and Game Theory which are applied to human-robot interactions.

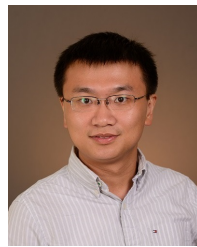


Mukesh Ghimire received his B.S. in Mechanical Engineering with minors in Computer Science and Mathematics from the University of Mississippi in 2021. He is a Ph.D. student and research assistant in the Design Informatics Lab, Arizona State University. His research interests include Game Theory, Artificial Intelligence and Reinforcement Learning.



Zhe Xu received the B.S. and M.S. degrees in Electrical Engineering from Tianjin University, Tianjin, China, in 2011 and 2014, respectively. He received the Ph.D. degree in Electrical Engineering at Rensselaer Polytechnic Institute, Troy, NY, in 2018. He is currently an assistant professor in the School for Engineering of Matter, Transport, and Energy at Arizona State University. Before joining ASU, he was a postdoctoral researcher at the Oden Institute for Computational Engineering and Sciences at the University of Texas at Austin, Austin, TX.

His research interests include formal methods, autonomous systems, control systems, and reinforcement learning.



Wenlong Zhang received the B.Eng. degree (Hons.) in control science and engineering from Harbin Institute of Technology, Harbin, China, in 2010, and the M.S. degree in mechanical engineering in 2012, the M.A. degree in statistics in 2013, and Ph.D. degree in mechanical engineering in 2015, all from the University of California, Berkeley, CA, USA. He is currently an Associate Professor in the School of Manufacturing Systems and Networks at ASU, where he directs the ASU Robotics and Intelligent Systems (RISE) Lab. His research interests include

dynamic systems and control, interactive robotics, and human-machine collaboration.



Yi Ren is an Associate Professor in Mechanical Engineering at Arizona State University. He received his Ph.D. in Mechanical Engineering from the University of Michigan Ann Arbor in 2012 and his B.Eng. degree in Automotive Engineering from Tsinghua University in 2007. From 2012 to 2014 he was a post-doctoral researcher at the University of Michigan. Dr. Ren's current research focuses on safety in AI-enabled engineering systems. He won the Best Paper Award at the 2015 ASME International Design and Engineering Technical Confer-

ences (IDETC).